Research Article

Ronaldo Walter Laureano and José Luis Mantari*

Layerwise generalized formulation solved *via* a boundary discontinuous method for multilayered structures. Part 1: Plates

https://doi.org/10.1515/cls-2024-0020
received July 05, 2024; accepted October 23, 2024

Abstract: This article presents for the very first time a layerwise bending analytical solution for cross-ply laminated composite plates with clamped boundary conditions at all edges. The displacement field is implemented within the framework of the Carrera unified formulation at a layer level by employing Legendre polynomials. The governing equations are obtained by using the principle of virtual displacements statement. This work utilizes the boundary-discontinuous double Fourier series to provide analytical solutions. The high accuracy of the proposed solution is demonstrated by comparing the results with three-dimensional finite-element model (FEM) solutions of multilayered and sandwich plates for various side-to-thickness ratios. In conclusion, the highly accurate proposed solution might be used as a benchmark problem for new analytical or FEMs.

Keywords: CUF, layerwise theory, clamped, boundary discontinuous, analytical

1 Introduction

Composite multilayered plates have become ubiquitous in a diverse range of engineering applications, including aerospace, mechanical, biomedical, marine, automotive design, and civil structures. Indeed, composite plates boast a multitude of advantageous mechanical properties, such as a high stiffness-to-weight ratio, low density, and exceptional resistance to both impact and corrosion. The expanding applications of composite material structures underscore the need for the advancement of precise and efficient numerical methods capable of accurately simulating the intricate behavior exhibited by laminated composites.

Three-dimensional (3D) theories grounded in elasticity theory result in significant challenges when dealing with laminate plates. Pagano [1,2] analyzed the deformation behaviors of cross-ply laminated plates using 3D elasticity theory. Ren [3] obtained closed-form solutions for special types of simply-supported angle-ply laminated plates under transverse loading by employing the bending theory presented in [4,5]. However, 3D solutions have some extra challenges when different than simply-supported boundary conditions are a concern. Then, a simplified two-dimensional (2D) mathematical model for the elasticity theory of laminated composites is an alternative solution for such difficult problems related to free or clamped boundary conditions.

Regarding 2D models, classical theories such as the works of Kirchhoff [6], Love [7], and the so-called classical lamination theory [8] are suitable only for thin laminated plates as they neglect the out-of-plane strains. The first-order shear deformation theory (FSDT) [9,10], accounting for constant transverse shear components, incorporates a shear correction factor, leading to improved results for both thick and thin plates. Nevertheless, the calculation of the shear correction factor poses a challenge, as it is contingent on the lamination sequence, loading conditions, and boundary conditions. Higher-order shear deformation theories (HSDTs) overcome the limitations of FSDT by the introduction of higher-order terms in their displacement field. HSDTs can be formulated by expanding the displacement components in both polynomial and non-polynomial series of the thickness coordinate, allowing for flexibility in achieving any desired order. Generally, based on the variable description, two approaches stand out: the equivalent single layer (ESL) and the layerwise (LW) models. The ESL approach assumes that the number of unknowns is independent of the number of layers, whereas the LW approach posits that each layer has its own set of variables.

* **Corresponding author: José Luis Mantari**, Faculty of Mechanical Engineering, Universidad de Ingenieria y Tecnologia (UTEC) Engineering and Technology, Jr. Medrano Silva 165, Barranco, Lima, Peru, e-mail: jmantari@utec.edu.pe, tel: +51 964358966
Ronaldo Walter Laureano: Faculty of Mechanical Engineering, Universidad de Ingenieria y Tecnologia (UTEC) Engineering and Technology, Jr. Medrano Silva 165, Barranco, Lima, Peru

In fact, ESL models present a lower computational cost; however, they encounter challenges in accurately reproducing the characteristic Zig-Zag effects observed in laminates. Conversely, LW models offer nearly 3D predictive capabilities, albeit at the cost of increased computational expense.

A variety of ESL models have been developed. Reddy [11] presented a simple HSDT for multilayered simply-supported plates considering a parabolic distribution for transverse shear strains. Murakami [12] proposed his so-called Zig-Zag theory by adding a local Zig-Zag function in the displacement field. Touratier [13] introduced an innovative approach for expanding the thickness coordinate to derive a plate formulation that accounts for cosine shear stress distribution and free boundary conditions. Li and Liu [14] presented an independent-layer generalized Zig-Zag theory to study the static behavior of simply-supported cross-ply laminated plates. Carrera [15] presented a historical review of the Zig-Zag theories for multilayered plates and shells. Regarding LW theories, Reddy [16] developed his well-known 2D generalized LW theory, where Lagrangian interpolation functions are utilized to satisfy the C_z^0 continuity. Furthermore, Ferreira [17,18] implemented an LW theory in a mesh-free method known as the multiquadric radial basis functions to analyze laminated composite and sandwich plates. Comprehensive reviews of current ESL and LW models are available in the referenced literature [19–22].

Two decades ago, Carrera [23,24] introduced a unified theory for multilayered structures known as the Carrera unified formulation (CUF). This formulation enables researchers to employ diverse series expansions of the unknown variables along the thickness in a compact manner. In [24], Carrera utilized both the principle of virtual displacements (PVDs) and Reissner's mixed variational theorem (RMVT) statements to formulate ESL and LW theories, respectively. Carrera and Ciuffreda [25] conducted a comparison of approximately 40 CUF-based theories for multilayered composites and sandwich plates subjected to transverse pressure, considering various in-plane load distributions. Ferreira *et al.* [26] integrated CUF with a radial basis function collocation technique to conduct static and free vibration analyses of thick isotropic and cross-ply laminated plates employing FSDT and HSDT. Ramos *et al.* [27] employed a modified non-polynomial CUF-based displacement field for the analysis of simply-supported laminated plates under thermal loads. Trigonometric, exponential, and hyperbolic series were employed to build the cross-section functions for refined beam models [28]. Carrera *et al.* [29] presented solutions for mechanical responses of angle-ply laminated plates by using refined FE models and Chebyshev expansions within the framework of CUF. Pagani *et al.* [30] adopted Lagrange polynomials and FE formulation under the ESL approach for modeling laminated structures. Recently, Petrolo *et al.* [31] and Carrera *et al.* [32] proposed hierarchical expansions built by using Jacobi polynomials to analyze multilayered beams, plates, and shells. Demasi [33] developed an interesting extension of CUF to the so-called generalized unified formulation. Further literature on CUF models can be explored in the literature [34–39].

The boundary-discontinuous double Fourier series was formulated by Chaudhuri [40,41]. This solution methodology was applied successfully in static and free vibration analysis of plates and panels in previous studies [42–52]. Chaudhuri and Kabir [53,54] presented analytical solutions for the static deformations and rotations of cross-ply laminated and isotropic rectangular plates under SS1, SS2, and C4-type boundary conditions. Oktem and Chaudhuri [55,56] presented a Levy-type analytical solution to the problem of deformation of a general cross-ply thick rectangular plate HSDT under mixed boundary conditions. In another study [57], the same authors studied the effect of end clamping on the response of a thick laminated plate under C3-type clamped boundary conditions while keeping the in-plane end constraint unaltered. Oktem *et al.* [58] explored the static behavior of functionally graded (FG) plates and doubly curved shells using Reddy's HSDT [11]. Canales and Mantari [59,60] provided analytical closed-form solutions of fully clamped laminated beams by employing ESL-based CUF and the boundary-discontinuous method. Recently, Laureano *et al.* [61,62] presented an extension of previous unified formulations to study fully clamped laminated and FG plates based on ESL models.

In this work, closed-form solutions for the static behavior of fully clamped cross-ply laminated and sandwich plates are presented. The principal innovation in this article lies in the adoption of a CUF-based model under an LW approach employing Legendre polynomials along with the boundary-discontinuous generalized double Fourier method to solve complex boundary problems in an analytical manner. Indeed, this hybrid methodology is expressed at a layer level for the very first time in the literature. The strong form of governing equations is obtained through the PVD. Thus, the strong and unified formulation is utilized to provide quasi-3D numerical results. The results clearly highlight the distinct advantages and superior performance of the current approach in accurately capturing displacement behavior and stress distributions across the entire thickness.

The structure of the article is outlined as follows: Section 2 comprehensively details the analytical modeling, including the analytical solution. Section 3 showcases the numerical results obtained through the proposed approach

for various benchmarks. Finally, Section 4 addresses the main conclusions drawn from the study.

2 Analytical modeling

Consider the laminated composite plate in Figure 1 where the geometry and coordinate system are shown. N_l denotes the number of layers, whereas integer k, which can be used as a subscript or superscript, indicates the layer number starting from the bottom of the plate. x and y are the plate middle surface coordinates, while z denotes the thickness direction. The structure is situated within the following region:

$$0 \le x \le a,\ 0 \le y \le b,\ -\frac{h}{2} \le z \le \frac{h}{2}.$$

Unlike ESL description, an LW approach uses local variables for each layer:

$$-\frac{h_k}{2} \le z_k \le \frac{h_k}{2}, \tag{1}$$

$$-1 \le \zeta_k \le 1, \tag{2}$$

where z_k is the physical coordinate of the k-layer whose thickness is h_k. Additionally, ζ_k is a non-dimensioned layer coordinate with $\zeta_k = \frac{2z_k}{h_k}$.

2.1 Elastic stress–strain relations

A generalized displacement vector $\boldsymbol{u^k}$ for each layer is given as follows:

$$\boldsymbol{u}^k = \{u^k\ v^k\ w^k\}^T. \tag{3}$$

The stress and strain components are expressed in vectorial form with no loss of generality:

$$\boldsymbol{\sigma}^k = \{\sigma_{xx}^k\ \sigma_{yy}^k\ \tau_{xy}^k\ \tau_{xz}^k\ \tau_{yz}^k\ \sigma_{zz}^k\}^T, \tag{4}$$

$$\boldsymbol{\varepsilon}^k = \{\varepsilon_{xx}^k\ \varepsilon_{yy}^k\ \gamma_{xy}^k\ \gamma_{xz}^k\ \gamma_{yz}^k\ \varepsilon_{zz}^k\}^T, \tag{5}$$

where σ_{ii}^k, $(i = x, y, z)$ and τ_{ij}^k $(i \neq j)$ denote normal and shear stress components, respectively. Similar notation is used for strains where $\boldsymbol{\varepsilon}_{ii}^k$, $(i = x, y, z)$ and $\boldsymbol{\gamma}_{ij}^k$ $(i \neq j)$ denote normal and shear strains, respectively.

The stress and strain vectors in Eqs. (4) and (5) are divided into in-plane $(\boldsymbol{\sigma}_p^k, \boldsymbol{\varepsilon}_p^k)$ and out-of-plane $(\boldsymbol{\sigma}_n^k, \boldsymbol{\varepsilon}_n^k)$ components:

$$\boldsymbol{\sigma}_p^k = \{\sigma_{xx}^k\ \sigma_{yy}^k\ \tau_{xy}^k\}^T, \tag{6a}$$

$$\boldsymbol{\sigma}_n^k = \{\ \tau_{xz}^k\ \tau_{yz}^k\ \sigma_{zz}^k\ \}^T, \tag{6b}$$

$$\boldsymbol{\varepsilon}_p^k = \{\ \varepsilon_{xx}^k\ \varepsilon_{yy}^k\ \gamma_{xy}^k\ \}^T, \tag{7a}$$

$$\boldsymbol{\varepsilon}_n^k = \{\ \gamma_{xz}^k\ \gamma_{yz}^k\ \varepsilon_{zz}^k\ \}^T. \tag{7b}$$

The in-plane $\boldsymbol{\varepsilon}_p^k$ and out-plane $\boldsymbol{\varepsilon}_n^k$ are linearly related to the displacement $\boldsymbol{u}^k$:

$$\boldsymbol{\varepsilon}_p^k = \boldsymbol{D}_p \boldsymbol{u}^k, \tag{8a}$$

$$\boldsymbol{\varepsilon}_n^k = (\boldsymbol{D}_{np} + \boldsymbol{D}_{nz})\boldsymbol{u}^k. \tag{8b}$$

$\boldsymbol{D}_p$, $\boldsymbol{D}_{np}$, and $\boldsymbol{D}_{nz}$ denote in-plane and out-of-plane differential operators:

$$\boldsymbol{D}_p = \begin{bmatrix} \frac{\partial}{\partial x} & 0 & 0 \\ 0 & \frac{\partial}{\partial y} & 0 \\ \frac{\partial}{\partial y} & \frac{\partial}{\partial x} & 0 \end{bmatrix},\ \boldsymbol{D}_{np} = \begin{bmatrix} 0 & 0 & \frac{\partial}{\partial x} \\ 0 & 0 & \frac{\partial}{\partial y} \\ 0 & 0 & 0 \end{bmatrix},$$
$$\boldsymbol{D}_{nz} = \begin{bmatrix} \frac{\partial}{\partial z} & 0 & 0 \\ 0 & \frac{\partial}{\partial z} & 0 \\ 0 & 0 & \frac{\partial}{\partial z} \end{bmatrix}. \tag{9}$$

The linear stress–strain relations are as follows:

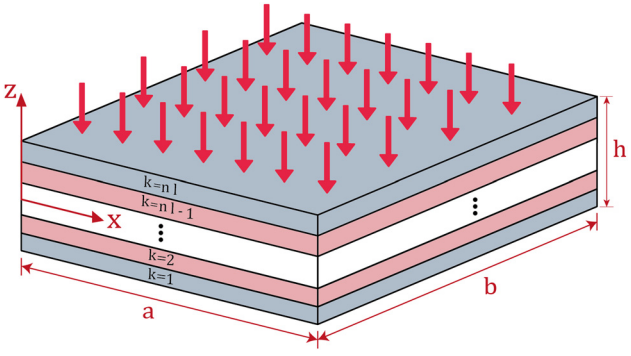

Figure 1: Coordinate frame of the plate model.

Table 1: Thickness expansion functions

F_τ	$F(\zeta_k)$
F_b	$\frac{\zeta_k - 1}{2}$
F_2	$\frac{3\zeta_k^2 - 3}{2}$
F_3	$\frac{5\zeta_k^3 - 5\zeta_k}{2}$
F_4	$\frac{35\zeta_k^4 - 42\zeta_k^2 + 7}{8}$
F_t	$\frac{\zeta_k + 1}{2}$

Table 2: List of materials

Material	E_1	E_2	E_3	G_{12}	G_{13}	G_{23}	ν_{12}	ν_{13}	ν_{23}
	(GPa)								
1	172.5	6.9	6.9	3.45	3.45	1.38	0.25	0.25	0.25
2	6.9	6.9	6.9	3.45	3.45	1.38	0.25	0.25	0.25
3	172.5	6.9	69	3.45	3.45	1.38	0.25	0.25	0.25

$$\boldsymbol{\sigma}_p^k = \tilde{\boldsymbol{C}}_{pp}^k\, \boldsymbol{\varepsilon}_p^k + \tilde{\boldsymbol{C}}_{pn}^k\, \boldsymbol{\varepsilon}_n^k, \tag{10a}$$

$$\boldsymbol{\sigma}_n^k = \tilde{\boldsymbol{C}}_{np}^k\, \boldsymbol{\varepsilon}_p^k + \tilde{\boldsymbol{C}}_{nn}^k\, \boldsymbol{\varepsilon}_n^k. \tag{10b}$$

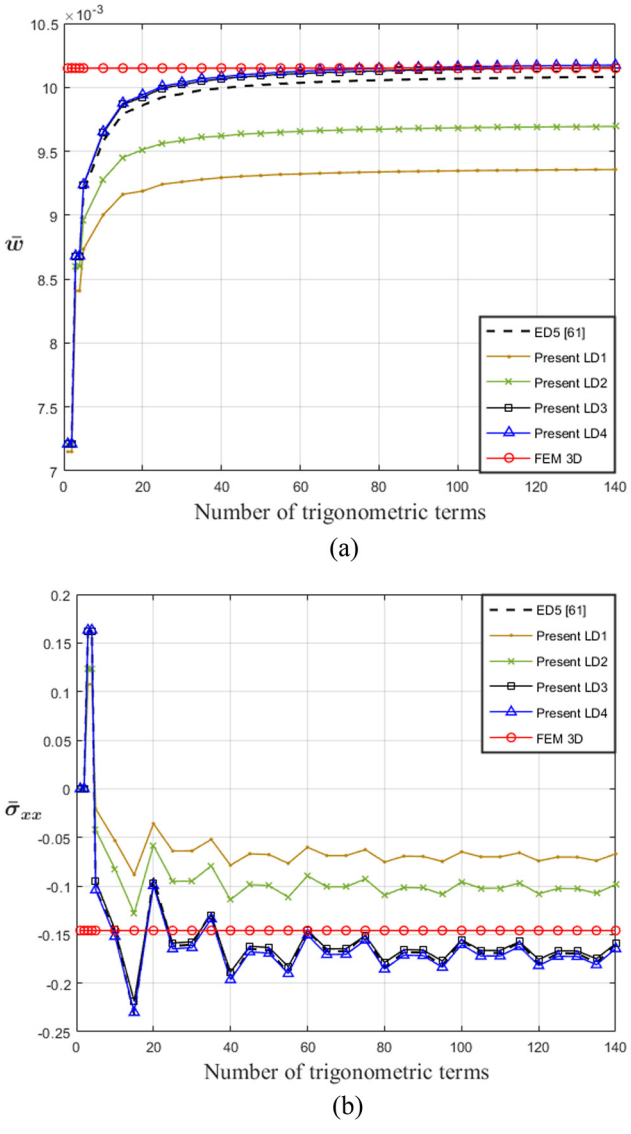

Figure 2: Convergence of nondimensional (a) transversal displacement $\bar{w}\left(\frac{a}{4}, \frac{b}{4}, 0\right)$ and (b) in-plane normal stress $\bar{\sigma}_{xx}\left(\frac{a}{4}, \frac{b}{4}, \frac{h}{2}\right)$ of a Problem I thick square plate $\left(\frac{a}{h} = 4\right)$.

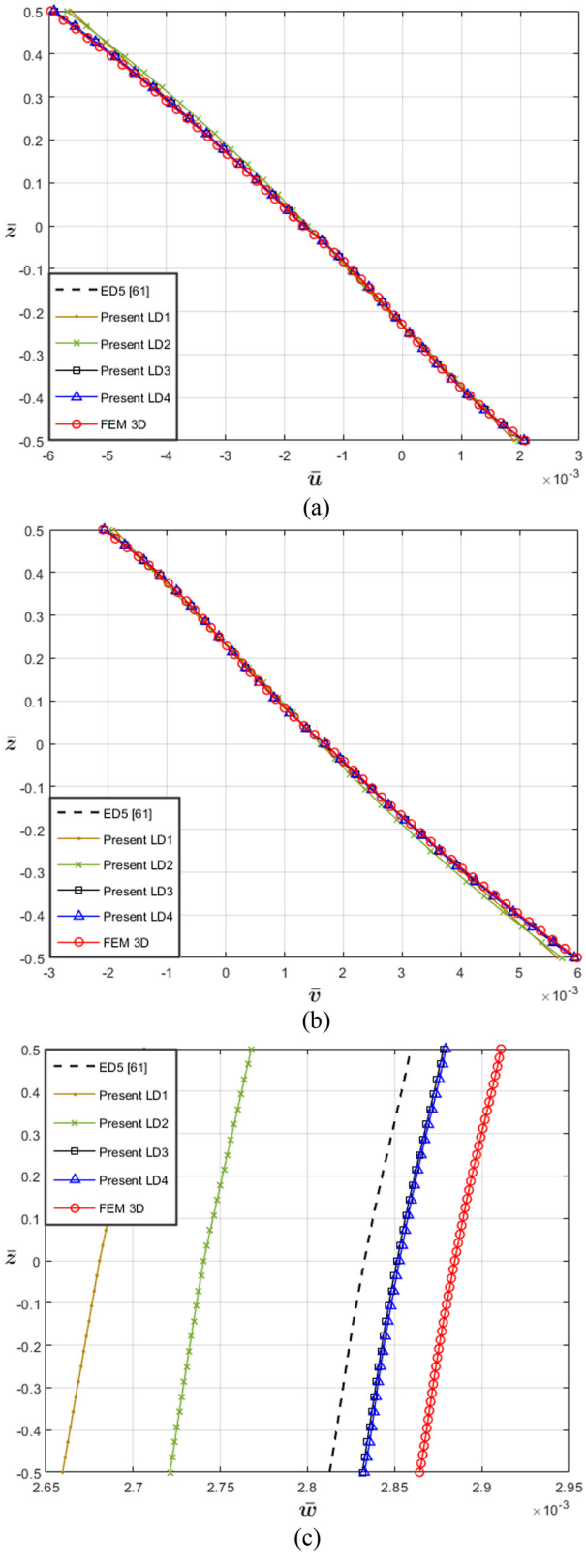

Figure 3: (a)–(c). Problem I. Through-the-thickness variation of displacement components at the point $\left(x = \frac{a}{4}, y = \frac{b}{4}\right)$ of a moderately thick laminated plate $\left(\frac{a}{h} = 10\right)$.

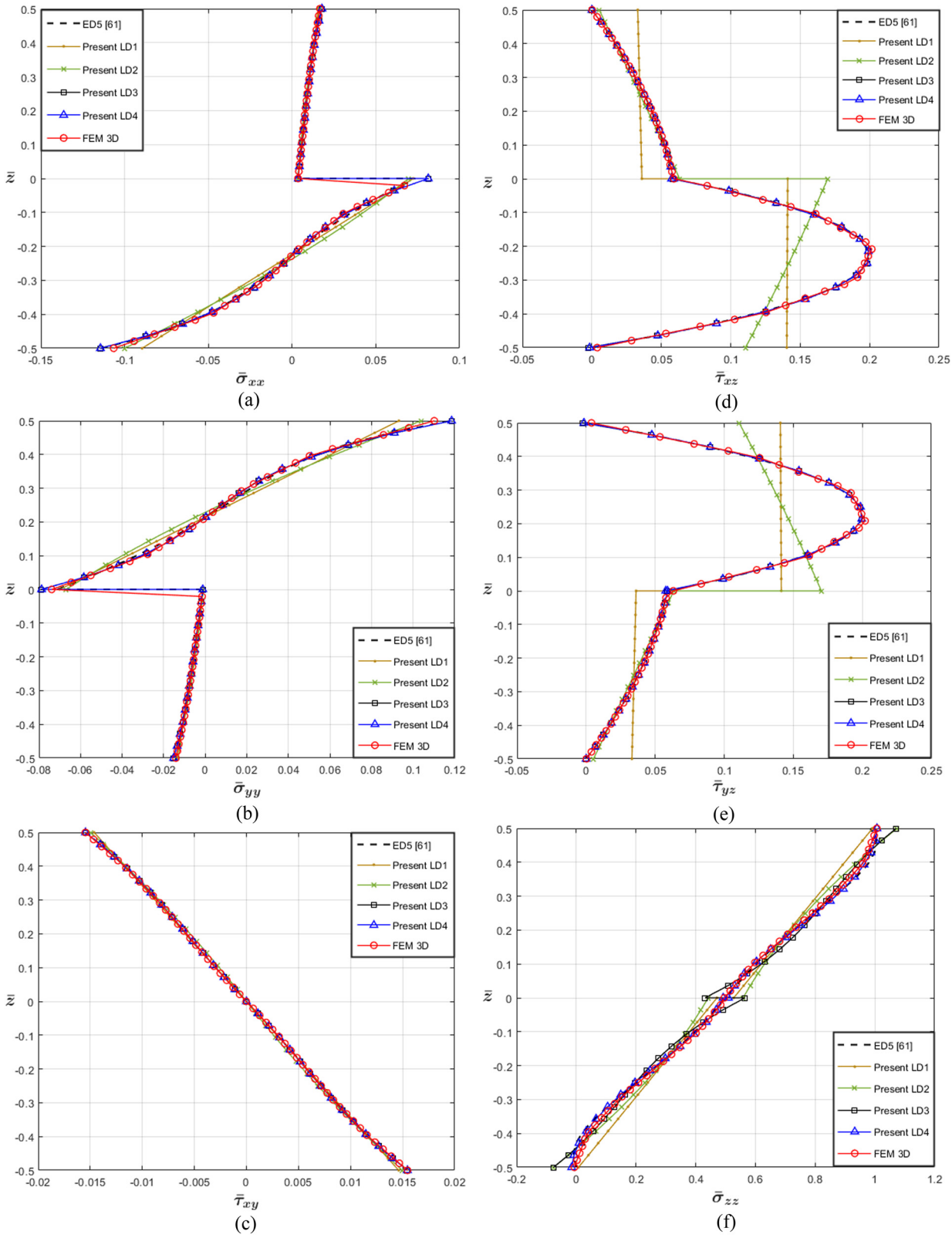

Figure 4: (a)–(f). Problem I. Through-the-thickness variation of stress components at the point $\left(x = \frac{a}{4}, y = \frac{b}{4}\right)$ of a moderately thick laminated plate $\left(\frac{a}{h} = 10\right)$.

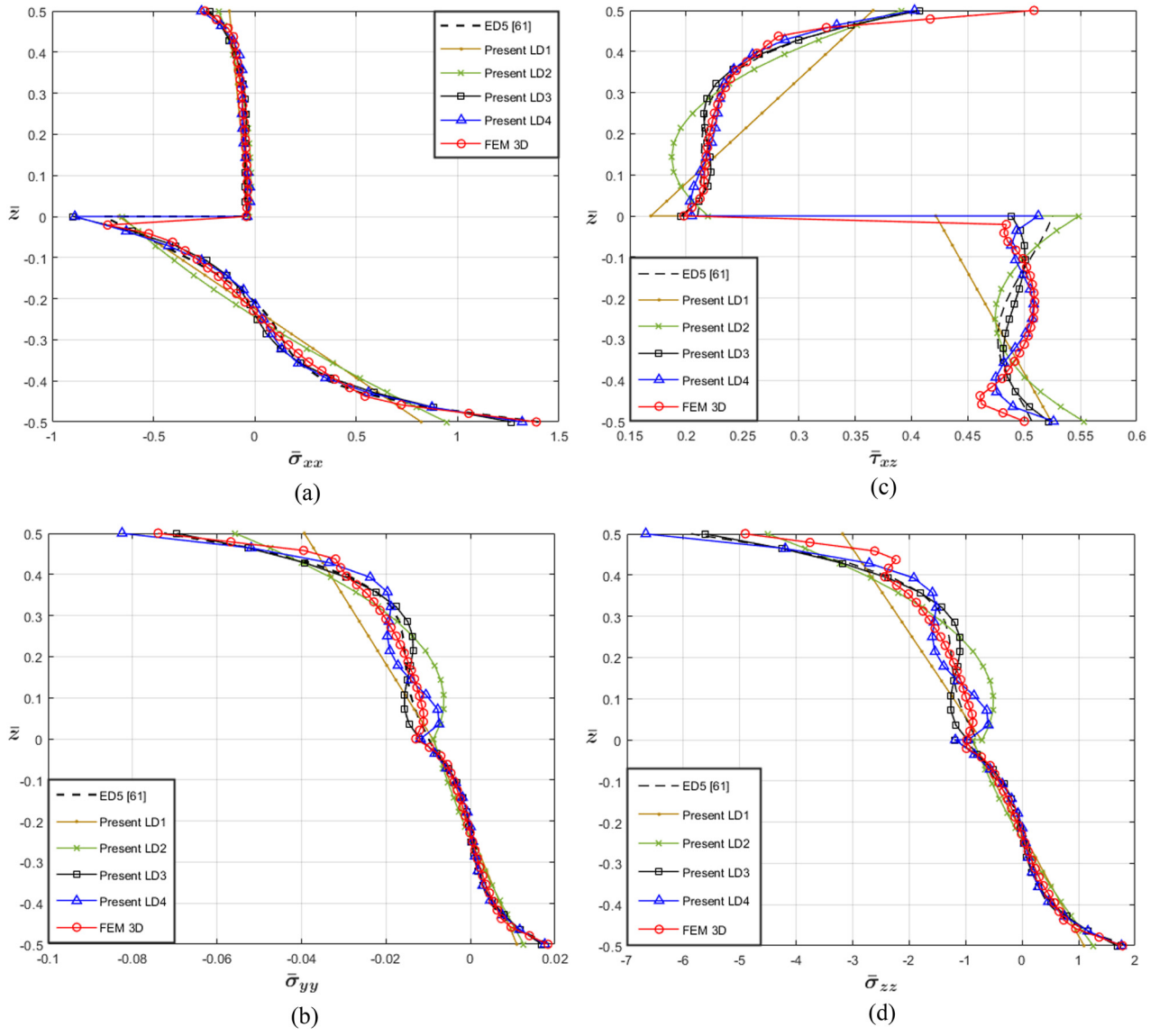

Figure 5: (a)–(d). Problem I. Through-the-thickness distribution of in-plane and out-of-plane stress components at a clamped edge $\left(x = 0, y = \frac{b}{2}\right)$ of a moderately thick $\left(\frac{a}{h} = 10\right)$ square plate.

Here, $\tilde{\boldsymbol{C}}_{pp}^{k}$, $\tilde{\boldsymbol{C}}_{pn}^{k}$, $\tilde{\boldsymbol{C}}_{np}^{k}$, and $\tilde{\boldsymbol{C}}_{nn}^{k}$ are matrices of material coefficients of the k-layer. In this work, orthotropic materials are employed:

$$\tilde{\boldsymbol{C}}_{pp}^{k} = \begin{bmatrix} \tilde{C}_{11}^{k} & \tilde{C}_{12}^{k} & 0 \\ \tilde{C}_{12}^{k} & \tilde{C}_{22}^{k} & 0 \\ 0 & 0 & \tilde{C}_{66}^{k} \end{bmatrix}, \quad \tilde{\boldsymbol{C}}_{nn}^{k} = \begin{bmatrix} \tilde{C}_{55}^{k} & 0 & 0 \\ 0 & \tilde{C}_{44}^{k} & 0 \\ 0 & 0 & \tilde{C}_{33}^{k} \end{bmatrix},$$
$$\tilde{\boldsymbol{C}}_{pn}^{k} = \tilde{\boldsymbol{C}}_{np}^{k^{T}} = \begin{bmatrix} 0 & 0 & \tilde{C}_{13}^{k} \\ 0 & 0 & \tilde{C}_{23}^{k} \\ 0 & 0 & 0 \end{bmatrix}. \tag{11}$$

For the sake of brevity, the relations between the coefficients of $\tilde{\boldsymbol{C}}$ and the engineering constants of the material are not reported here; they can be found in the textbook by Carrera [35]. It is assumed that orthotropic laminae are oriented on planes parallel to the (x, y) plane. As a limitation, the boundary-discontinuous double Fourier method is applicable exclusively to cross-ply laminated structures, where laminae are oriented at 0° or 90° from the X-axis, similar to Navier-type solutions.

2.2 Displacement field

According to Carrera [23,24], an LW model based on CUF can be written for the vector displacement $\boldsymbol{u}^{k} = \{u^{k}\ v^{k}\ w^{k}\}^{T}$ as follows:

$$u^k = F_b(\zeta)u_b^k(x,y) + F_r(\zeta)u_r^k(x,y) + F_t(\zeta)u_t^k(x,y), \quad (12a)$$

$$v^k = F_b(\zeta)v_b^k(x,y) + F_r(\zeta)v_r^k(x,y) + F_t(\zeta)v_t^k(x,y), \quad (12b)$$

$$w^k = F_b(\zeta)w_b^k(x,y) + F_r(\zeta)w_r^k(x,y) + F_t(\zeta)w_t^k(x,y), \quad (12c)$$

where b and t denote the bottom and the top of the plate. Eqs. (12a)–(12c) can also be written in a compact form:

$$\begin{aligned} \boldsymbol{u}^k &= F_\tau(\zeta)\,\boldsymbol{u}_\tau^k(x,y), \\ \delta\boldsymbol{u}^k &= F_s(\zeta)\,\delta\boldsymbol{u}_s^k(x,y),\ \tau,s = t,\ b,\ r\ (r = 2,\ 3\ ,\ldots,\ N), \end{aligned} \quad (13)$$

where the thickness functions $\boldsymbol{F}_\tau$ and $\boldsymbol{F}_s$ are defined in Table 1.

The interlaminar displacement continuity is a priori imposed as follows:

$$u_t^k = u_b^{k+1},\ k = 1, N_l - 1, \quad (14a)$$

$$v_t^k = v_b^{k+1},\ k = 1, N_l - 1, \quad (14b)$$

$$w_t^k = w_b^{k+1},\ k = 1, N_l - 1. \quad (14c)$$

2.3 Governing equations

The displacement approach is formulated in terms of $\boldsymbol{u}^k$ by variationally imposing the equilibrium *via* the PVD statement. Therefore, the strong form of governing, differential equations, and the related natural boundary conditions are obtained. The PVD can be written in its static version as

$$\delta\boldsymbol{L}_{\text{int}} = \delta\boldsymbol{L}_{\text{ext}}, \quad (15)$$

where $\boldsymbol{L}_{\text{int}}$ represents the internal elastic work, $\boldsymbol{L}_{\text{ext}}$ is for the work done by the external forces, and, as before, $\boldsymbol{\delta}$ stands for a virtual variation.

Taking into account strain–displacement relations (Eqs. (8a) and (8b)), stress–strain relations (Eqs. (10a) and (10b)), the compact form of CUF (Eq. (13)), and integrating by parts to obtain strong form equations [24]:

$$\begin{aligned} \delta L_{\text{int}} &= \sum_{k=1}^{N_l} \int_{\Omega_k} \int_{A_k} (\delta\boldsymbol{\varepsilon}_p^{k^T}\boldsymbol{\sigma}_p^k + \delta\boldsymbol{\varepsilon}_n^{k^T}\boldsymbol{\sigma}_n^k)\mathrm{d}z\ \mathrm{d}\Omega_k \\ &= \sum_{k=1}^{N_l} \int_{\Omega_k} \delta\boldsymbol{u}_s^{kT}\boldsymbol{K}^{k\tau s}\boldsymbol{u}_\tau^k\ \mathrm{d}\Omega_k + \int_{\Gamma_k} \delta\boldsymbol{u}_s^{kT}\boldsymbol{\Pi}^{k\tau s}\boldsymbol{u}_\tau^k\ \mathrm{d}\Gamma_k, \end{aligned} \quad (16)$$

where $\boldsymbol{K}^{k\tau s}$ is the stiffness matrix in the form of the fundamental nuclei and $\boldsymbol{\Pi}^{k\tau s}$ is the matrix of the natural boundary conditions. The components of $\boldsymbol{K}^{k\tau s}$ and $\boldsymbol{\Pi}^{k\tau s}$ are provided in Appendix A, where a generic parameter in the thickness direction is used and is defined below:

$$J_{ab}^{k\tau,\phi s,\theta} = \int_{A_k} \tilde{C}_{ab}^k F_{\tau,\phi} F_{s,\theta}\mathrm{d}z, \quad (17)$$

where $\tau_{,\phi}s_{,\theta}$ indicate which functions are to be used, whether $\boldsymbol{F}_\tau$ and $\boldsymbol{F}_s$ or their derivatives $\boldsymbol{F}_{\tau,z}$, $\boldsymbol{F}_{s,z}$. Moreover, a, b stand for indexes of the employed coefficient of $\tilde{\boldsymbol{C}}^k$.

The virtual variation in external loadings is expressed as follows:

$$\delta L_{\text{ext}} = \sum_{k=1}^{N_l} \int_{\Omega_k} \delta\boldsymbol{u}_s^{kT}\boldsymbol{P}_s^k\ \mathrm{d}\Omega_k, \quad (18)$$

Table 3: Problem I. Numerical results of displacements and stress components at the point $\left(x = \frac{a}{4},\ y = \frac{b}{4}\right)$ for different values of a/h

a/h	Model	$10^2\bar{u}_{z=\frac{h}{2}}$	$10^2\bar{v}_{z=\frac{h}{2}}$	$10^2\bar{w}_{z=0}$	$\bar{\sigma}_{xx_{z=\frac{h}{2}}}$	$\bar{\sigma}_{yy_{z=\frac{h}{2}}}$	$10\bar{\tau}_{xy_{z=\frac{h}{2}}}$	$10\bar{\tau}_{xz\,z=0}$	$10\bar{\tau}_{yz_{z=0}}$	$\bar{\sigma}_{zz\,z=0}$
4	LD1	−0.703	0.732	0.935	−0.074	0.101	−0.133	1.480	0.477	0.284
	LD2	−0.776	0.805	0.969	−0.108	0.141	−0.152	1.758	0.763	0.452
	LD3	−0.835	0.866	1.015	−0.176	0.215	−0.172	0.699	0.754	0.539
	LD4	−0.835	0.866	1.017	−0.182	0.222	−0.172	0.792	0.756	0.490
	FEM 3D	−0.843	0.873	1.025	−0.156	0.191	−0.170	0.729	0.802	0.493
	ED5 [61]	−0.839	0.869	1.008	−0.180	0.220	−0.172	0.722	0.754	0.498
10	LD1	−0.562	0.564	0.268	−0.090	0.093	−0.146	1.410	0.362	0.471
	LD2	−0.569	0.572	0.274	−0.100	0.104	−0.150	1.698	0.635	0.442
	LD3	−0.591	0.593	0.285	−0.114	0.118	−0.155	0.583	0.591	0.565
	LD4	−0.591	0.593	0.285	−0.114	0.119	−0.155	0.574	0.590	0.492
	FEM 3D	−0.597	0.599	0.289	−0.106	0.110	−0.155	0.591	0.632	0.495
	ED5 [61]	−0.591	0.594	0.283	−0.114	0.118	−0.155	0.584	0.587	0.5
50	LD1	−0.486	0.486	0.139	−0.096	0.097	−0.171	1.245	0.325	5.493
	LD2	−0.489	0.489	0.139	−0.097	0.097	−0.172	1.489	0.568	0.350
	LD3	−0.490	0.490	0.140	−0.098	0.098	−0.172	0.517	0.518	0.625
	LD4	−0.490	0.490	0.140	−0.098	0.098	−0.172	0.517	0.518	0.477
	FEM 3D	−0.489	0.489	0.137	−0.094	0.094	−0.172	0.533	0.534	0.485
	ED5 [61]	−0.486	0.486	0.135	−0.097	0.097	−0.173	0.515	0.515	0.495

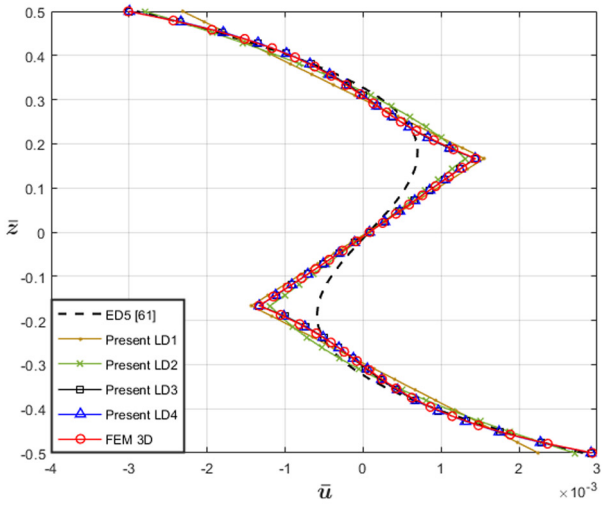

(a)

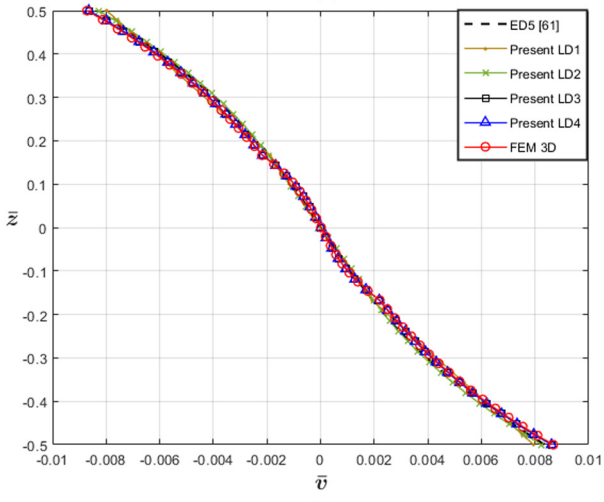

(b)

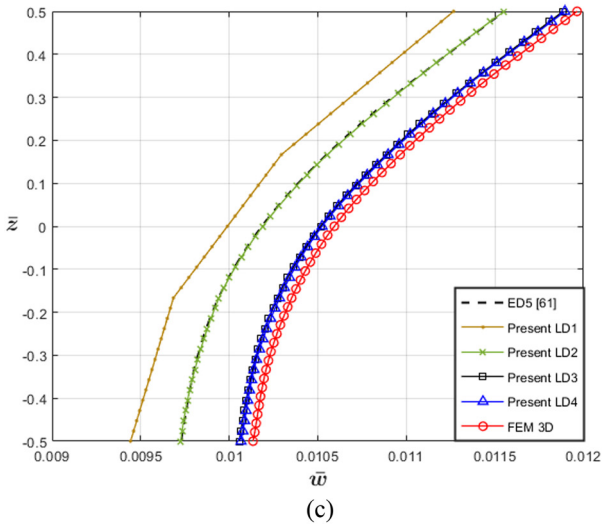

(c)

Figure 6: (a)–(c). Problem II. Through-the-thickness variation of displacement components at the point $\left(x = \frac{a}{4}, y = \frac{b}{4}\right)$ of a thick case $\left(\frac{a}{h} = 4\right)$.

where $\boldsymbol{P}_s^k = \left[0\ 0\ F_{s_{\left(z=\frac{h}{2}\right)}} q_z\right]^T$ is the external load applied at the top surface $\left(z = \frac{h}{2}\right)$ of the plate.

In a compact form, replacing Eqs. (13) and (15) in Eqs. (12a)–(12c), the following system of linear algebraic equations holds:

$$\delta \boldsymbol{u}_s^{kT} : \boldsymbol{K}^{k\tau s}\, \boldsymbol{u}_\tau^k = \boldsymbol{P}_s^k. \tag{19}$$

2.4 Boundary conditions

Geometric boundary conditions for simply-supported plates in terms of the displacement variables given in Eqs. (12a)–(12c) are expressed as

$$u_{\tau,x}^k(0, y) = 0, \tag{20a}$$

$$u_{\tau,x}^k(a, y) = 0, \tag{20b}$$

$$v_{\tau,y}^k(x, 0) = 0, \tag{20c}$$

$$v_{\tau,y}^k(x, b) = 0, \tag{20d}$$

$$w_\tau^k(0, y) = 0, \tag{20e}$$

$$w_\tau^k(a, y) = 0, \tag{20f}$$

$$w_\tau^k(x, 0) = 0, \tag{20g}$$

$$w_\tau^k(x, b) = 0. \tag{20h}$$

In addition, if the clamped boundary conditions are considered at the four edges (CCCC), the following conditions are added:

$$u_\tau^k(0, y) = 0, \tag{21a}$$

$$u_\tau^k(a, y) = 0, \tag{21b}$$

$$v_\tau^k(x, 0) = 0, \tag{21c}$$

$$v_\tau^k(x, b) = 0. \tag{21d}$$

However, for clamped edges, the conditions in Eqs. (20a)–(20d) changed to inequalities:

$$u_{\tau,x}^k(0, y) \neq 0, \tag{22a}$$

$$u_{\tau,x}^k(a, y) \neq 0, \tag{22b}$$

$$v_{\tau,y}^k(x, 0) \neq 0, \tag{22c}$$

$$v_{\tau,y}^k(x, b) \neq 0. \tag{22d}$$

2.5 Boundary-discontinuous solution

In order to fulfill the clamped boundary conditions stated in Eqs. (21a) and (21b) and (22a) and (22b), the boundary-

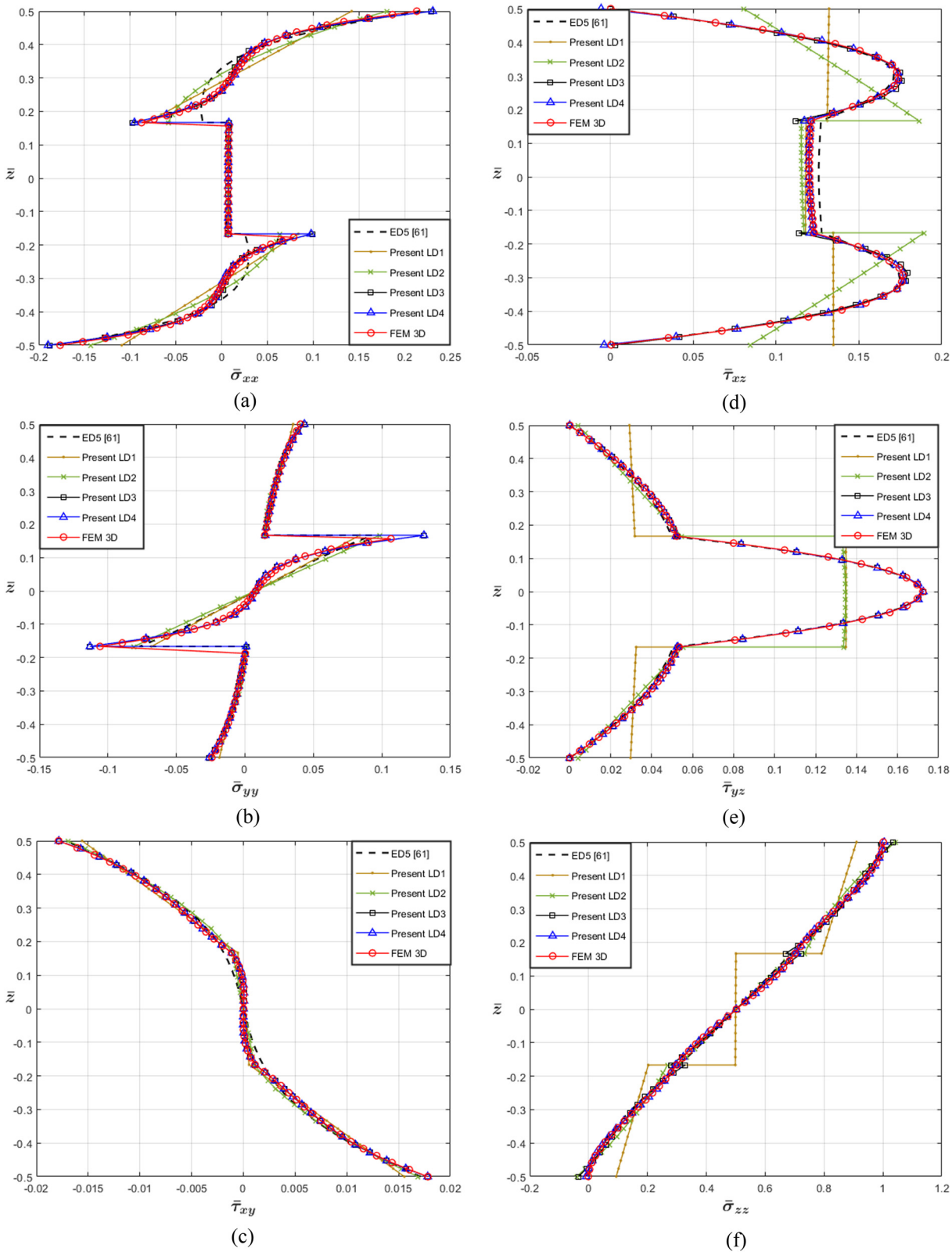

Figure 7: (a)–(f). Problem II. Through-the-thickness variation of stress components at the point $\left(x = \frac{a}{4}, y = \frac{b}{4}\right)$ of a thick case $\left(\frac{a}{h} = 4\right)$.

Table 4: Problem II. Numerical results of displacements and stress components at the point $\left(x = \frac{a}{4},\ y = \frac{b}{4}\right)$ for different values of a/h

a/h	Model	$10^2\bar{u}_{z=\frac{h}{2}}$	$10^2\bar{v}_{z=-\frac{h}{2}}$	$10^2\bar{w}_{z=0}$	$\bar{\sigma}_{xx_{z=\frac{h}{2}}}$	$10\bar{\sigma}_{yy_{z=\frac{h}{2}}}$	$10\bar{\tau}_{xy_{z=\frac{h}{2}}}$	$10\bar{\tau}_{xz_{z=0}}$	$10^2\bar{\tau}_{yz_{z=0}}$	$\bar{\sigma}_{zz_{z=0}}$
4	LD1	−0.231	0.794	0.999	−0.109	0.352	−0.156	1.179	13.482	0.500
	LD2	−0.280	0.823	1.019	−0.143	0.413	−0.169	1.155	13.459	0.499
	LD3	−0.300	0.861	1.052	−0.188	0.433	−0.178	1.198	17.247	0.501
	LD4	−0.300	0.861	1.052	−0.190	0.434	−0.178	1.199	17.256	0.501
	FEM 3D	−0.301	0.868	1.059	−0.177	0.406	−0.179	1.202	17.232	0.502
	ED5 [61]	−0.290	0.836	1.018	−0.177	0.423	−0.172	1.257	17.189	0.502
10	LD1	−0.164	0.397	0.256	−0.094	0.160	−0.102	1.994	6.671	0.501
	LD2	−0.178	0.405	0.262	−0.108	0.166	−0.107	1.979	6.780	0.500
	LD3	−0.179	0.409	0.266	−0.112	0.171	−0.107	1.982	9.090	0.500
	LD4	−0.179	0.409	0.267	−0.112	0.172	−0.107	1.982	9.092	0.500
	FEM 3D	−0.181	0.411	0.269	−0.105	0.161	−0.107	1.991	8.955	0.501
	ED5 [61]	−0.176	0.393	0.256	−0.108	0.165	−0.103	2.019	8.627	0.501
50	LD1	−0.148	0.111	0.067	−0.062	0.073	−0.056	2.622	0.171	0.498
	LD2	−0.148	0.112	0.067	−0.063	0.072	−0.056	2.623	0.176	0.498
	LD3	−0.148	0.112	0.068	−0.064	0.072	−0.056	2.631	0.195	0.498
	LD4	−0.148	0.112	0.068	−0.064	0.072	−0.056	2.631	0.195	0.498
	FEM 3D	−0.150	0.113	0.069	−0.060	0.069	−0.056	2.642	0.164	0.500
	ED5 [61]	−0.148	0.111	0.067	−0.063	0.071	−0.056	2.636	0.160	0.498

discontinuous double Fourier series is used. The assumed solutions and their derivatives will be replaced in Eq. (19) to furnish a linear system of equations. Based on the studies of Chaudhuri [40,41], the displacement variables u_τ^k, v_τ^k, and w_τ^k are expanded as follows:

$$u_\tau^k = \sum_{m=0}^{m}\sum_{n=1}^{n} U_{\tau mn}^k \cos(\alpha x)\sin(\beta y), \quad 0 < x < a;\ 0 \le y \le b, \tag{23a}$$

$$v_\tau^k = \sum_{m=1}^{m}\sum_{n=0}^{n} V_{\tau mn}^k \sin(\alpha x)\cos(\beta y), \quad 0 \le x \le a;\ 0 < y < b, \tag{23b}$$

$$w_\tau^k = \sum_{m=1}^{m}\sum_{n=1}^{n} W_{\tau mn}^k \sin(\alpha x)\sin(\beta y), \quad 0 \le x \le a;\ 0 \le y \le b. \tag{23c}$$

The load q_z is also expanded in Fourier series:

$$q_z = \sum_{m=1}^{m}\sum_{n=1}^{n} Q_{mn}\sin(\alpha x)\sin(\beta y),\ 0 \le x \le a;\ 0 \le y \le b, \tag{23d}$$

where

$$U_{\tau mn}^k = \frac{4}{ab}\int_0^b\int_0^a u_\tau^k \cos(\alpha x)\sin(\beta y)\mathrm{d}x\mathrm{d}y, \tag{24a}$$

$$V_{\tau mn}^k = \frac{4}{ab}\int_0^b\int_0^a v_\tau^k \sin(\alpha x)\cos(\beta y)\mathrm{d}x\mathrm{d}y, \tag{24b}$$

$$(W_{\tau mn}^k, Q_{mn}) = \frac{4}{ab}\int_0^b\int_0^a (w_\tau^k, q_z)\sin(\alpha x)\sin(\beta y)\mathrm{d}x\mathrm{d}y, \tag{24c}$$

$$\alpha = \frac{m\pi}{a}, \tag{24d}$$

$$\beta = \frac{n\pi}{b}. \tag{24e}$$

These assumed solutions introduce $[N_l(\mathrm{Nu}-1)+1](3mn+m+n)$ unknown variables where m and n represent the wave number of each trigonometric term in Eqs. (23a)–(23d) and (24a)–(24e). The load q_z is also expanded using a Fourier series in Eq. (23d) to analyze different types of loads such as distributed load, hydrostatic load, and localized load. Moreover, the explicit form of the differential equations in Eq. (19) can be expressed as follows:

$$\delta u_s^k:\ J_{55}^{k\tau,_z s,_z}\boldsymbol{u}_{\boldsymbol{\tau}}^{\boldsymbol{k}} - J_{11}^{k\tau s}\boldsymbol{u}_{\boldsymbol{\tau,xx}}^{\boldsymbol{k}} - J_{66}^{k\tau s}\boldsymbol{u}_{\boldsymbol{\tau,yy}}^{\boldsymbol{k}} - (J_{12}^{k\tau s} + J_{66}^{k\tau s})\boldsymbol{v}_{\boldsymbol{\tau,xy}}^{\boldsymbol{k}} + (J_{55}^{k\tau s,_z} - J_{13}^{k\tau,_z s})\boldsymbol{w}_{\boldsymbol{\tau,x}}^{\boldsymbol{k}} = 0, \tag{25a}$$

$$\delta v_s^k:\ -(J_{12}^{k\tau s} + J_{66}^{k\tau s})\boldsymbol{u}_{\boldsymbol{\tau,xy}}^{\boldsymbol{k}} + J_{44}^{k\tau,_z s,_z}\boldsymbol{v}_{\boldsymbol{\tau}}^{\boldsymbol{k}} - J_{66}^{k\tau s}\boldsymbol{v}_{\boldsymbol{\tau,xx}}^{\boldsymbol{k}} - J_{22}^{k\tau s}\boldsymbol{v}_{\boldsymbol{\tau,yy}}^{\boldsymbol{k}} + (J_{44}^{k\tau s,_z} - J_{23}^{k\tau,_z s})\boldsymbol{w}_{\boldsymbol{\tau,y}}^{\boldsymbol{k}} = 0, \tag{25b}$$

$$\delta w_s^k:\ (J_{13}^{k\tau s,_z} - J_{55}^{k\tau,_z s})\boldsymbol{u}_{\boldsymbol{\tau,x}}^{\boldsymbol{k}} + (J_{23}^{k\tau s,_z} - J_{44}^{k\tau,_z s})\boldsymbol{v}_{\boldsymbol{\tau,y}}^{\boldsymbol{k}} + J_{33}^{k\tau,_z s,_z}\boldsymbol{w}_{\boldsymbol{\tau}}^{\boldsymbol{k}} - J_{55}^{k\tau s}\boldsymbol{w}_{\boldsymbol{\tau,xx}}^{\boldsymbol{k}} - J_{44}^{k\tau s}\boldsymbol{w}_{\boldsymbol{\tau,yy}}^{\boldsymbol{k}} = F_s\, Q_{mn}. \tag{25c}$$

From Eqs. (25a) to (25c), the derivatives of the displacement variables (u_τ^k, v_τ^k, w_τ^k) need to be calculated. Besides, these derivatives must also satisfy the discontinuities specified in Eqs. (22a) and (22b). In the next lines, the core aspects

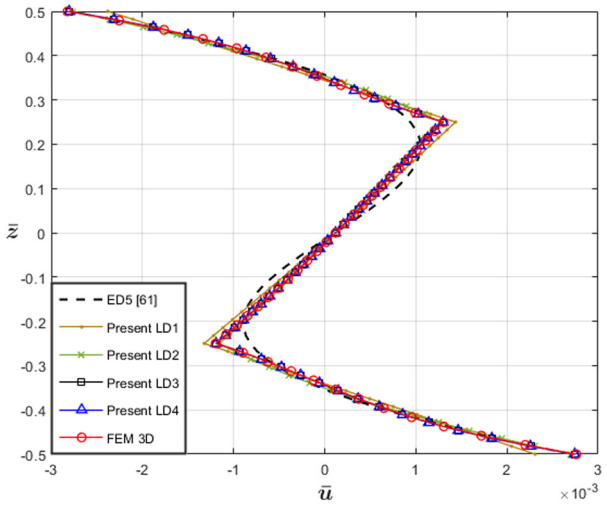

(a)

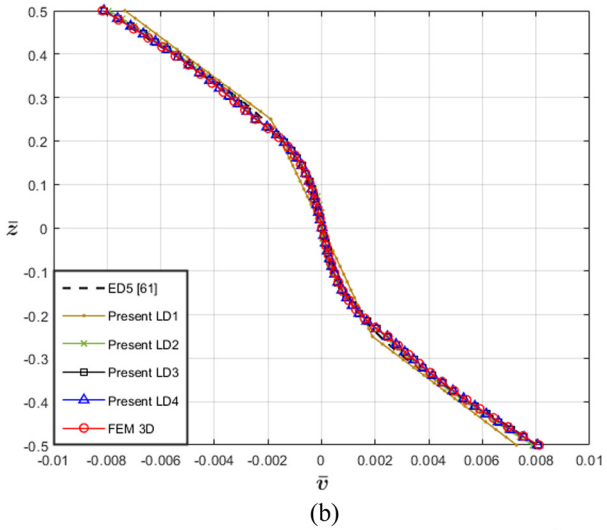

(b)

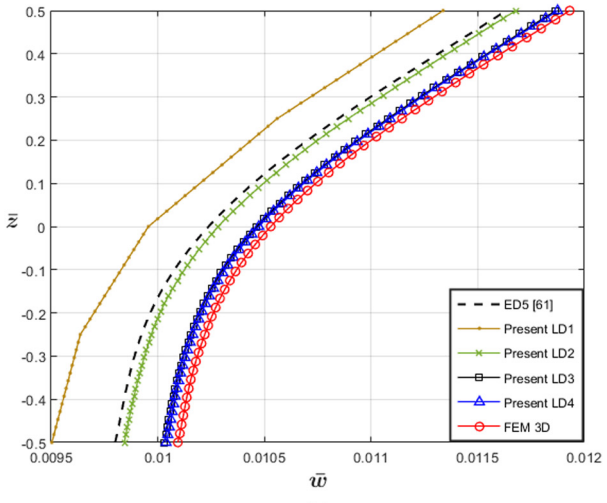

(c)

Figure 8: (a)–(c). Problem III. Through-the-thickness variation of displacement components at the point $\left(x = \frac{a}{4}, y = \frac{b}{4}\right)$ of a thick case $\left(\frac{a}{h} = 4\right)$.

of the proposed approach and its procedure are explained. For instance, according to Eqs. (22a) and (22b), $u^k_{\tau,x}$ is forced to vanish at $x = 0$ and $x = a$ whereas $v^k_{\tau,y}$ at $y = 0$ and $y = b$. Likewise, for further differentiation, if a function presents discontinuities, the derivative of the Fourier series is not necessarily the same as the Fourier series of the derivative of the function. In that case, $u^k_{\tau,x}$ is expanded in Fourier series:

$$u^k_{\tau,x} = \sum_{m=1}^{m}\sum_{n=1}^{n} U^k_{\tau mn,x}\sin(\alpha x)\sin(\beta y), \quad 0 < x < a;\ 0 \le y \le b, \tag{26a}$$

where $U^k_{\tau mn,x}$ is the Fourier term associated with the Fourier series of $u^k_{\tau,x}$:

$$U^k_{\tau mn,x} = \frac{4}{ab}\int_0^b\int_0^a u^k_{\tau,x}\sin(\alpha x)\sin(\beta y)\mathrm{d}x\mathrm{d}y. \tag{26b}$$

Then, integrating Eqs. (26a) and (26b) by parts and using the vanishing boundary conditions given in Eqs. (21a) and (21b):

$$U^k_{\tau mn,x} = \frac{2}{b}\int_0^b\left(\frac{2}{a}u^k_\tau\sin(\alpha x)|_{x=0}^{x=a} - \alpha\frac{2}{a}\int_0^a u^k_\tau\cos(\alpha x)\mathrm{d}x\right)\sin(\beta y)\mathrm{d}y, \tag{27a}$$

$$U^k_{\tau mn,x} = -\alpha\frac{4}{ab}\int_0^b\int_0^a u^k_{\tau,x}\cos(\alpha x)\sin(\beta y)\mathrm{d}x\mathrm{d}y, \tag{27b}$$

$$U^k_{\tau mn,x} = -\alpha U^k_{\tau mn}, \tag{27c}$$

replacing Eq. (27c) in Eq. (23a):

$$u^k_{\tau,x} = -\alpha\sum_{m=1}^{m}\sum_{n=1}^{n} U^k_{\tau mn}\sin(\alpha x)\sin(\beta y), \quad 0 < x < a;\ 0 \le y \le b. \tag{28}$$

Eqs. (26a) and (26b) show that $u^k_{\tau,x}$ can be obtained through term-by-term differentiation.

Next, the calculation of $u^k_{\tau,xx}$ is made. The Fourier series of $u^k_{\tau,xx}$ is given by

$$u^k_{\tau,xx} = \frac{1}{2}\sum_{n=1}^{n}\bar{a}^k_{\tau_n}\sin(\beta y) + \sum_{m=1}^{m}\sum_{n=1}^{n} U^k_{\tau mn,xx}\cos(\alpha x)\sin(\beta y), \quad 0 < x < a;\ 0 \le y \le b, \tag{29a}$$

where $U^k_{\tau mn,xx}$ is the Fourier term associated with the Fourier series of $u^k_{\tau,xx}$:

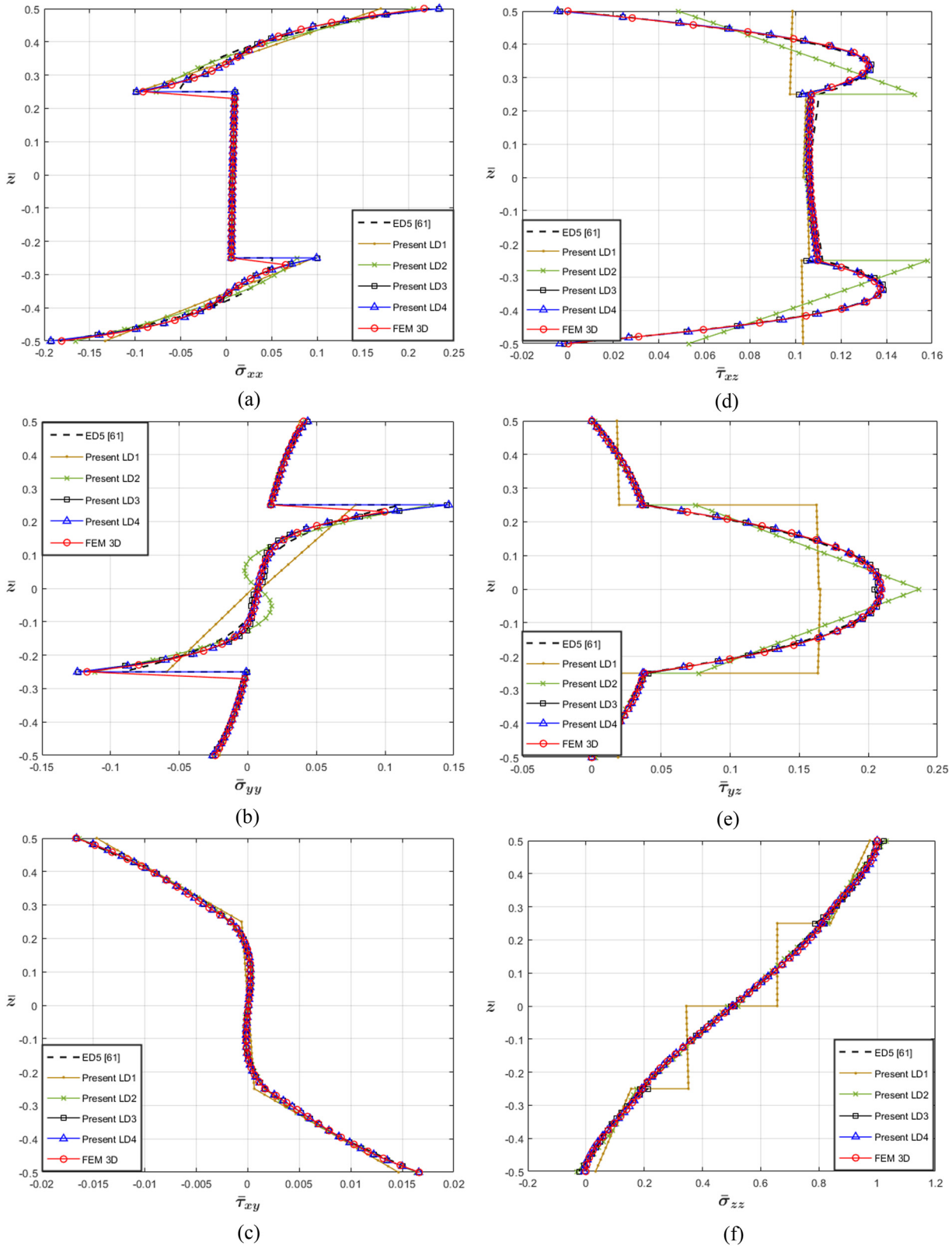

Figure 9: (a)–(f). Problem III. Through-the-thickness variation of stress components at the point $\left(x = \frac{a}{4}, y = \frac{b}{4}\right)$ of a thick case $\left(\frac{a}{h} = 4\right)$.

Table 5: Problem III. Numerical results of displacements and stress components at the point $\left(x = \frac{a}{4},\ y = \frac{b}{4}\right)$ for different values of a/h

a/h	Model	$10^2\bar{u}_{z=\frac{h}{2}}$	$10^2\bar{v}_{z=-\frac{h}{2}}$	$10^2\bar{w}_{z=0}$	$10^2\bar{\sigma}_{xx\,z=\frac{h}{2}}$	$10^2\bar{\sigma}_{yy\,z=\frac{h}{2}}$	$10^2\bar{\tau}_{xy\,z=\frac{h}{2}}$	$10^2\bar{\tau}_{xz\,z=0}$	$10^2\bar{\tau}_{yz\,z=0}$	$\bar{\sigma}_{zz\,z=0}$
4	LD1	−0.238	0.727	0.996	−13.309	3.780	−1.468	10.512	16.523	0.345
	LD2	−0.277	0.788	1.028	−16.593	4.202	−1.638	10.488	23.682	0.487
	LD3	−0.281	0.805	1.046	−19.265	4.335	−1.664	10.596	20.420	0.511
	LD4	−0.280	0.805	1.047	−19.277	4.362	−1.664	10.609	20.910	0.502
	FEM 3D	−0.282	0.811	1.053	−18.081	4.058	−1.668	10.636	20.956	0.504
	ED5 [61]	−0.278	0.800	1.024	−18.338	4.243	−1.653	10.670	20.990	0.505
10	LD1	−0.145	0.362	0.247	−9.330	1.344	−0.901	15.240	11.650	0.348
	LD2	−0.155	0.371	0.255	−10.403	1.442	−0.937	15.567	18.702	0.467
	LD3	−0.155	0.373	0.256	−10.541	1.462	−0.935	15.468	16.434	0.507
	LD4	−0.155	0.373	0.257	−10.573	1.471	−0.935	15.471	16.349	0.499
	FEM 3D	−0.156	0.376	0.259	−9.840	1.354	−0.937	15.533	16.411	0.501
	ED5 [61]	−0.154	0.368	0.251	−10.338	1.420	−0.926	15.627	16.087	0.501
50	LD1	−0.135	0.128	0.063	−5.995	0.547	−0.627	19.994	2.921	1.530
	LD2	−0.136	0.128	0.063	−6.061	0.540	−0.628	20.210	4.687	0.468
	LD3	−0.136	0.128	0.063	−6.101	0.541	−0.628	20.148	4.109	0.508
	LD4	−0.136	0.128	0.063	−6.106	0.541	−0.628	20.148	4.104	0.495
	FEM 3D	−0.138	0.129	0.064	−5.775	0.516	−0.629	20.236	4.226	0.502
	ED5 [61]	−0.136	0.127	0.063	−6.073	0.539	−0.627	20.171	4.062	0.498

$$U^k_{\tau mn,xx} = \frac{4}{ab}\int_0^b\int_0^a u^k_{\tau,xx}\cos(\alpha x)\sin(\beta y)\mathrm{d}x\mathrm{d}y. \tag{29b}$$

Then, integrating Eq. (27b) by parts, the following expression is obtained:

$$U^k_{\tau mn,xx} = \frac{2}{b}\int_0^b\left(\frac{2}{a}u^k_{\tau,x}\cos(\alpha x)|_{x=0}^{x=a} + \alpha\frac{2}{a}\int_0^a u^k_{\tau,x}\sin(\alpha x)\mathrm{d}x\right)\sin(\beta y)\mathrm{d}y. \tag{30}$$

Unlike Eq. (27a), in Eq. (30), there are no vanishing conditions for $u^k_{\tau,x}$ at $x = 0$ and $x = a$ according to Eqs. (22a) and (22b). Subsequently, grouping as follows:

$$U^k_{\tau mn,xx} = \frac{4}{ab}\int_0^b[(-1)^m u^k_{\tau,x}(a,y) - u^k_{\tau,x}(0,y)]\sin(\beta y)\mathrm{d}y + \alpha\frac{4}{ab}\int_0^b\int_0^a u^k_{\tau,x}\ \sin(\alpha x)\sin(\beta y)\mathrm{d}x\ \mathrm{d}y, \tag{31a}$$

$$U^k_{\tau mn,xx} = \frac{4}{ab}\int_0^b[(-1)^m u^k_{\tau,x}(a,y) - u^k_{\tau,x}(0,y)]\sin(\beta y)\mathrm{d}y\ + \alpha\ U^k_{\tau mn,x}, \tag{31b}$$

$$U^k_{\tau mn,xx} = \frac{4}{ab}\int_0^b[(-1)^m u^k_{\tau,x}(a,y) - u^k_{\tau,x}(0,y)]\sin(\beta y)\mathrm{d}y\ - \alpha^2\ U^k_{\tau mn}, \tag{31c}$$

replacing Eq. (31c) in Eq. (29a):

$$u^k_{\tau,xx} = \frac{1}{2}\sum_{n=1}^{n}\bar{a}^k_{\tau_n}\sin(\beta y) + \sum_{m=1}^{m}\sum_{n=1}^{n}[-\alpha^2\ U^k_{\tau mn} + \gamma_m\bar{a}^k_{\tau_n} + \psi_m\bar{b}^k_{\tau_n}]\cos(\alpha x)\sin(\beta y), \tag{32}$$

where $\bar{a}^k_{\tau_n}$, $\bar{b}^k_{\tau_n}$ introduce $[N_l(\mathrm{Nu}-1)+1](2n)$ new unknown variables. The definition of these constant coefficients is given by

$$(\bar{a}^k_{\tau_n}, \bar{b}^k_{\tau_n}) = \frac{4}{ab}\int_b^0[\pm u^k_{\tau,x}(a,y) - u^k_{\tau,x}(0,y)]\sin(\beta y)\mathrm{d}y. \tag{33}$$

In Eq. (33), $\bar{a}^k_{\tau_n}$ and $\bar{b}^k_{\tau_n}$ are directly related to the discontinuities of $u_{\tau,x}$ at the edges $x = 0$ and $x = a$. Furthermore, $u^k_{\tau,x}(0,y)$ and $u^k_{\tau,x}(a,y)$ can be expressed in terms of $\bar{a}^k_{\tau_n}$ and $\bar{b}^k_{\tau_n}$ as follows:

$$(u^k_{\tau,x}(0,y),\ u^k_{\tau,x}(a,y)) = -\frac{a}{4}\sum_{n=1}^{n}(\pm\bar{a}^k_{\tau_n} + \bar{b}^k_{\tau_n})\sin(\beta y). \tag{34}$$

γ_m and ψ_m are defined as

$$(\gamma_m, \psi_m) = \begin{cases}(1,0), & m = \text{even}\\ (0,1), & m = \text{odd}\end{cases}. \tag{35}$$

Subsequently, the first and second partial derivatives of v^k_τ are also required. Then, an analogous process is applied. The first partial derivative $v^k_{\tau,y}$ is given by

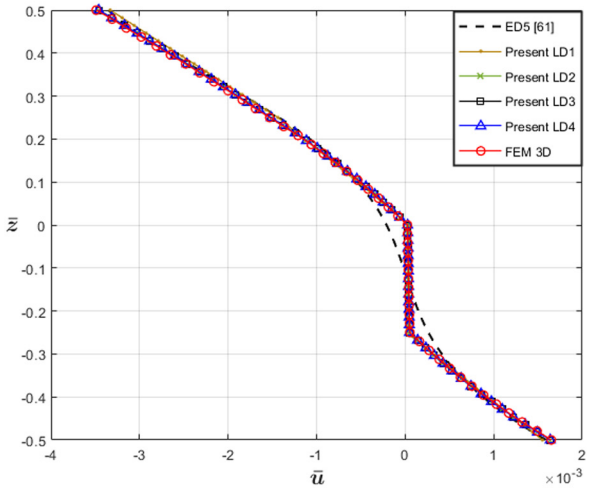

(a)

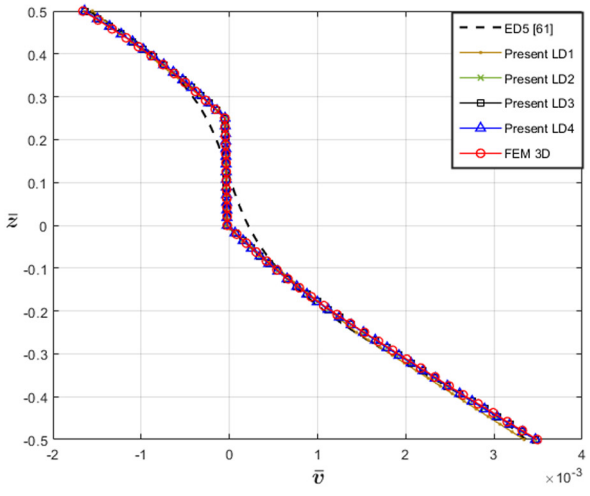

(b)

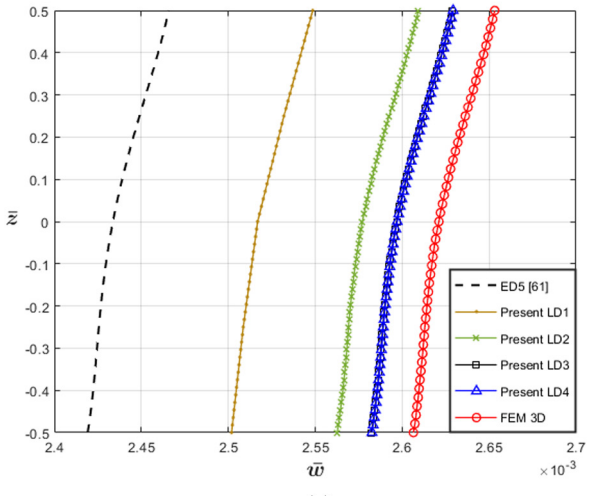

(c)

Figure 10: (a)–(c). Problem IV. Through-the-thickness variation of displacement components at the point $\left(x = \frac{a}{4}, y = \frac{b}{4}\right)$ of a moderately thick case $\left(\frac{a}{h} = 10\right)$.

$$v^k_{\tau,y} = -\sum_{m=1}^{m}\sum_{n=1}^{n} \beta V^k_{\tau mn} \sin(\alpha x)\sin(\beta y). \tag{36}$$

The second partial derivative $v^k_{\tau,yy}$ is written as follows:

$$v^k_{\tau,yy} = \frac{1}{2}\sum_{m=1}^{m} \bar{c}^k_{\tau_m} \sin(\alpha x) + \sum_{m=1}^{m}\sum_{n=1}^{n}[-\beta^2 V^k_{\tau mn} + \gamma_n \bar{c}^k_{\tau_m} + \psi_n \bar{d}^k_{\tau_m}]\sin(\alpha x)\cos(\beta y), \tag{37}$$

where $\bar{c}^k_{\tau_m}$ and $\bar{d}^k_{\tau_m}$ introduce $[N_l(\mathrm{Nu}-1)+1](2n)$ new unknown variables. These coefficients are given by

$$(\bar{c}^k_{\tau_m}, \bar{d}^k_{\tau_m}) = \frac{4}{ab}\int_a^0 [\pm v^k_{\tau,y}(x,b) - v^k_{\tau,y}(x,0)]\sin(\alpha x)\mathrm{d}x. \tag{38}$$

As in Eq. (34), the discontinuities of $v^k_{\tau,y}$ at the edges $y = 0$ and $y = b$ can be expressed as

$$(v^k_{\tau,y}(x,0), v^k_{\tau,y}(x,b)) = -\frac{b}{4}\sum_{m}^{m=1}(\pm\bar{c}^k_{\tau_m} + \bar{d}^k_{\tau_m})\sin(\alpha x). \tag{39}$$

γ_n and ψ_n are similar functions as Eq. (35).

The remaining partial derivatives can be obtained through term-by-term differentiation as they do not deal with discontinuities.

Later, the introduction of the displacement functions $u^k_\tau, v^k_\tau, w^k_\tau$ and their corresponding derivatives into Eq. (25) results in the following:

$$\begin{aligned}\sum_{m=1}^{m}\sum_{n=1}^{n} &\cos(\alpha x)\sin(\beta y)\{(\alpha^2 J^{k\tau s}_{11} + \beta^2 J^{k\tau s}_{66} + J^{k\tau,_z s,_z}_{55})\boldsymbol{U^k_{\tau mn}} \\ &- \alpha\beta(J^{k\tau s}_{12} + J^{k\tau s}_{66})\boldsymbol{V^k_{\tau mn}} + \alpha(J^{k\tau s,_z}_{55} - J^{k\tau,_z s}_{13})\boldsymbol{W^k_{\tau mn}} \\ &- J^{k\tau s}_{11}(\gamma_m \bar{\boldsymbol{a}}^{\boldsymbol{k}}_{\boldsymbol{\tau_n}} + \psi_m \bar{\boldsymbol{b}}^{\boldsymbol{k}}_{\boldsymbol{\tau_n}})\} = 0,\end{aligned} \tag{40a}$$

$$\begin{aligned}\sum_{m=1}^{m}\sum_{n=1}^{n} &\sin(\alpha x)\cos(\beta y)\{\alpha\beta(J^{k\tau s}_{12} + J^{k\tau s}_{66})\boldsymbol{U^k_{\tau mn}} \\ &+ (\alpha^2 J^{k\tau s}_{66} + \beta^2 J^{k\tau s}_{22} + J^{k\tau,_z s,_z}_{44})\boldsymbol{V^k_{\tau mn}} \\ &+ \beta(J^{k\tau s,_z}_{44} - J^{k\tau,_z s}_{23})\boldsymbol{W^k_{\tau mn}} - J^{k\tau s}_{22}(\gamma_n \bar{\boldsymbol{c}}^{\boldsymbol{k}}_{\boldsymbol{\tau_m}} + \psi_n \bar{\boldsymbol{d}}^{\boldsymbol{k}}_{\boldsymbol{\tau_m}})\} \\ &= 0,\end{aligned} \tag{40b}$$

$$\begin{aligned}\sum_{m=1}^{m}\sum_{n=1}^{n} &\sin(\alpha x)\sin(\beta y)\{\alpha(J^{k\tau,_z s}_{55} - J^{k\tau s,_z}_{13})\boldsymbol{U^k_{\tau mn}} \\ &+ \beta(J^{k\tau,_z s}_{44} - J^{k\tau s,_z}_{23})\boldsymbol{V^k_{\tau mn}} + (\alpha^2 J^{k\tau s}_{55} + \beta^2 J^{k\tau s}_{44} \\ &+ J^{k\tau,_z s,_z}_{33})\boldsymbol{W^k_{\tau mn}} - F_s Q_{mn}\} = 0,\end{aligned} \tag{40c}$$

$$\sum_{n=1}^{n}\sin(\beta y)\left\{(\beta^2 J^{k\tau s}_{66} + J^{k\tau,_z s,_z}_{55})\boldsymbol{U^k_{\tau 0 n}} - \frac{1}{2}J^{k\tau s}_{11}\,\bar{\boldsymbol{a}}^{\boldsymbol{k}}_{\boldsymbol{\tau_n}}\right\} = 0, \tag{40d}$$

$$\sum_{m=1}^{m}\sin(\alpha x)\left\{(\alpha^2 J^{k\tau s}_{66} + J^{k\tau,_z s,_z}_{44})\boldsymbol{V^k_{\tau m 0}} - \frac{1}{2}J^{k\tau s}_{22}\,\bar{\boldsymbol{c}}^{\boldsymbol{k}}_{\boldsymbol{\tau_m}}\right\} = 0. \tag{40e}$$

Until this point, Eqs. (40a)–(40e) provide only $[N_l(\mathrm{Nu}-1)+1](3mn+m+n)$ equations, whereas the

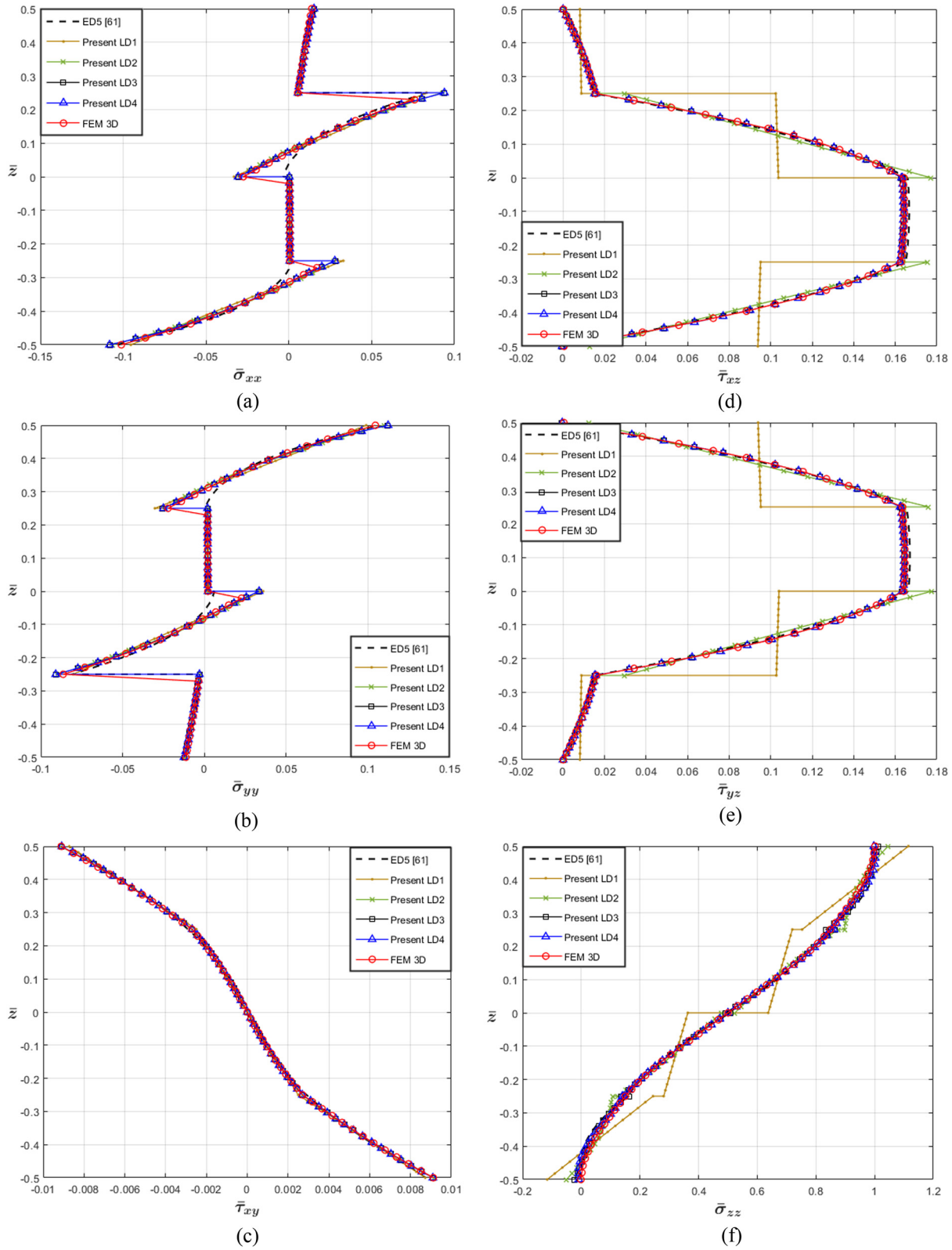

Figure 11: (a)–(f). Problem IV. Through-the-thickness variation of stress components at the point $\left(x = \frac{a}{4}, y = \frac{b}{4}\right)$ of a moderately thick case $\left(\frac{a}{h} = 10\right)$.

Table 6: Problem IV. Numerical results of displacements and stress components at the point $\left(x = \frac{a}{4},\ y = \frac{b}{4}\right)$ for different values of a/h

a/h	Model	$10^2\bar{u}_{z=\frac{h}{2}}$	$10^2\bar{v}_{z=-\frac{h}{2}}$	$10^2\bar{w}_{z=0}$	$10^2\bar{\sigma}_{xx_{z=\frac{h}{2}}}$	$10^2\bar{\sigma}_{yy_{z=\frac{h}{2}}}$	$10^2\bar{\tau}_{xy_{z=\frac{h}{2}}}$	$10^2\bar{\tau}_{xz_{z=0}}$	$10^2\bar{\tau}_{yz_{z=0}}$	$\bar{\sigma}_{zz_{z=0}}$
4	LD1	−0.764	0.767	1.030	−13.580	17.073	−1.569	12.525	13.001	0.356
	LD2	−0.795	0.801	1.051	−16.882	20.748	−1.690	12.297	17.082	0.498
	LD3	−0.813	0.818	1.075	−19.610	23.571	−1.721	12.560	12.293	0.516
	LD4	−0.813	0.819	1.076	−19.620	23.635	−1.720	12.566	12.717	0.502
	FEM 3D	−0.818	0.823	1.082	−18.416	21.970	−1.724	12.607	12.939	0.503
	ED5 [61]	−0.798	0.804	1.027	−18.925	22.918	−1.668	13.720	14.076	0.505
10	LD1	−0.333	0.334	0.252	−9.541	9.895	−0.872	16.442	10.398	0.363
	LD2	−0.346	0.347	0.258	−10.634	11.004	−0.913	16.429	17.758	0.477
	LD3	−0.346	0.347	0.260	−10.798	11.190	−0.909	16.334	16.318	0.509
	LD4	−0.346	0.347	0.260	−10.828	11.233	−0.909	16.335	16.329	0.500
	FEM 3D	−0.349	0.349	0.262	−10.118	10.455	−0.912	16.409	16.400	0.500
	ED5 [61]	−0.335	0.336	0.243	−10.326	10.686	−0.875	16.600	16.636	0.501
50	LD1	−0.189	0.189	0.068	−6.153	6.166	−0.763	14.210	8.876	1.415
	LD2	−0.190	0.190	0.069	−6.212	6.225	−0.765	14.289	15.310	0.463
	LD3	−0.190	0.190	0.069	−6.241	6.255	−0.765	14.231	14.233	0.519
	LD4	−0.190	0.190	0.069	−6.245	6.259	−0.765	14.231	14.229	0.498
	FEM 3D	−0.192	0.192	0.070	−5.959	5.972	−0.768	14.541	14.283	0.503
	ED5 [61]	−0.189	0.189	0.067	−6.197	6.211	−0.766	14.168	14.168	0.498

unknown variables are $[N_l(\mathrm{Nu}-1)+1](3mn+3m+3n)$. Hence, $[N_l(\mathrm{Nu}-1)+1](2m+2n)$ equations are required to match the number of variables. These remaining equations are provided by Eqs. (21a)–(21d).

Replacing Eq. (23a) in Eqs. (21a) and (21b), the following expressions are obtained:

$$\sum_{m=1,3,5,\ldots}^{\infty} \boldsymbol{U}_{\tau mn}^{k} = 0, \tag{41a}$$

$$\boldsymbol{U}_{\tau 0n}^{k} + \sum_{m=2,4,6,\ldots}^{\infty} \boldsymbol{U}_{\tau mn}^{k} = 0. \tag{41b}$$

Subsequently, Eq. (23b) can be replaced in Eqs. (21c) and (21d):

$$\sum_{n=1,3,5,\ldots}^{\infty} \boldsymbol{V}_{\tau mn}^{k} = 0, \tag{42a}$$

$$\boldsymbol{V}_{\tau m0}^{k} + \sum_{n=2,4,6,\ldots}^{\infty} \boldsymbol{V}_{\tau mn}^{k} = 0. \tag{42b}$$

Eqs. (41a), (41b), (42a), and (42b) generate the remaining $[N_l(\mathrm{Nu}-1)+1](2m+2n)$ equations for the solution. Thus, a complete solution is furnished.

3 Results and discussion

In this section, the accuracy of the proposed LW approach is assessed. Four cases of cross-ply laminated and sandwich plates under uniform distributed load have been selected. The clamped boundary condition is set at all four edges for all cases. Table 2 presents the mechanical properties of the materials employed in this study. The following dimensionless parameters are used for displacements and stresses:

$$(\bar{u}, \bar{v}) = \frac{E_2^{\mathrm{bottom}} h^2}{q_z a^3}(u, v),$$

$$\bar{w} = \frac{E_2^{\mathrm{bottom}} h^3}{q_z a^4} w,$$

$$(\bar{\sigma}_{xx}, \bar{\sigma}_{yy}, \bar{\tau}_{xy}) = \frac{h^2}{q_z a^2}(\sigma_{xx}, \sigma_{yy}, \tau_{xy}),$$

$$(\bar{\tau}_{xz}, \bar{\tau}_{yz}) = \frac{h}{q_z a}(\tau_{xz}, \tau_{yz}),$$

$$\bar{\sigma}_{zz} = \frac{1}{q_z}\sigma_{zz}.$$

To compare the results, FEM 3D results are presented. These were obtained by using ANSYS commercial code. For each scenario, ten brick elements per layer along the thickness are established. The code has been implemented in MATLAB, utilizing “sparse” as a matrix construction tool to enhance computational efficiency. Additionally, this article examines and compares the proposed LW approach with the work previously developed by Laureano *et al.* [61], which introduced theories based on the ESL approach. Besides, the out-of-plane stresses are calculated *via* Hooke’s law. Several LW theories are implemented, where “L”

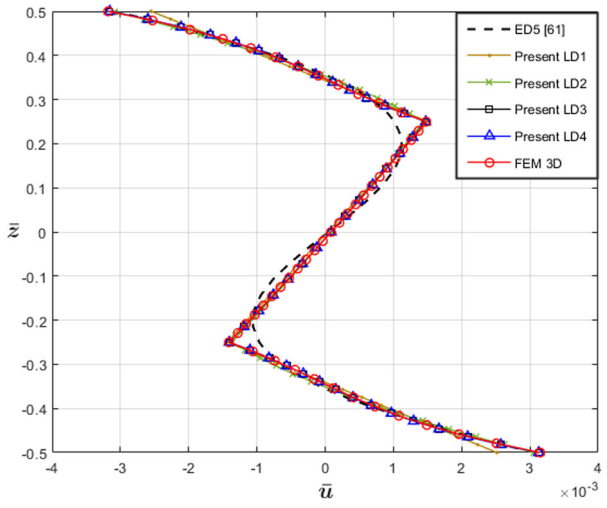

Figure 12: (a)–(c). Problem V. Through-the-thickness variation of displacement components at the point $\left(x = \frac{a}{4}, y = \frac{b}{4}\right)$ of a thick case $\left(\frac{a}{h} = 4\right)$.

represents the Layerwise approach, and "D" signifies the use of the displacement-based statement (PVD). The notation "LDN" indicates an Nth-order theory; for example, LD2 refers to a second-order theory, while LD4 represents a fourth-order theory.

3.1 Convergence analysis

The precision of the boundary-discontinuous method is significantly influenced by the number of trigonometric terms, denoted as m, n. To determine an appropriate value for m, n, Figure 2 illustrates the behavior of dimensionless transversal displacement and in-plane stress as m, n are incrementally varied. The plate in study is a cross-ply [0°/90°] moderately thick square plate whose layers are made of Material 1. From first-order (LD1) to fourth-order (LD4) model is plotted along with the reference FEM 3D solution and the ESL-based fifth-order theory (ED5) solution provided in [61]. Figure 2a shows the high accuracy of the present LD4 as it is closer to 3D FEM solution than ED5. In Figure 2b, the oscillatory pattern of $\bar{\sigma}_{xx}$ is noticeable, consistently approaching the FEM reference as the values of m, n increase. However, choosing larger values for m, n results in escalated computational costs. Therefore, for the forthcoming tables and figures, a value of 140 is selected for m, n, striking a balance between precision and the required computational resources.

3.2 Problem I. Two-layer antisymmetric square plate

For this initial problem, an antisymmetric cross-ply laminated [0°/90°] square plate made from Material 1 is examined. Figures 3 and 4 show the through-the-thickness distribution of displacements $(\bar{u}, \bar{v}, \bar{w})$ and stresses $(\bar{\sigma}_{xx}, \bar{\sigma}_{yy}, \bar{\tau}_{xy}, \bar{\tau}_{xz}, \bar{\tau}_{yz}, \bar{\sigma}_{zz})$ at the point $\left(\frac{a}{4}, \frac{b}{4}\right)$ of a moderately thick $\left(\frac{a}{h} = 10\right)$ plate. For this problem, a very close agreement is obtained in every stress profile. The results of LD3 and LD4 for the transversal displacement $\bar{w}$ are more accurate than ED5. Moreover, Figure 5 shows the in-plane $(\bar{\sigma}_{xx}, \bar{\sigma}_{yy})$ and out-of-plane $(\bar{\tau}_{xz}, \bar{\sigma}_{zz})$ stress profiles at a clamped edge $\left(x = 0, y = \frac{b}{2}\right)$. As illustrated, the current approach adeptly captures the in-plane stress distributions along with 3D FEM and ED5 solutions. However, in the case of $\bar{\tau}_{xz}$ profile, LD4 predicts more accurately than ED5 as its results closely align to the FEM 3D outcomes. Table 3

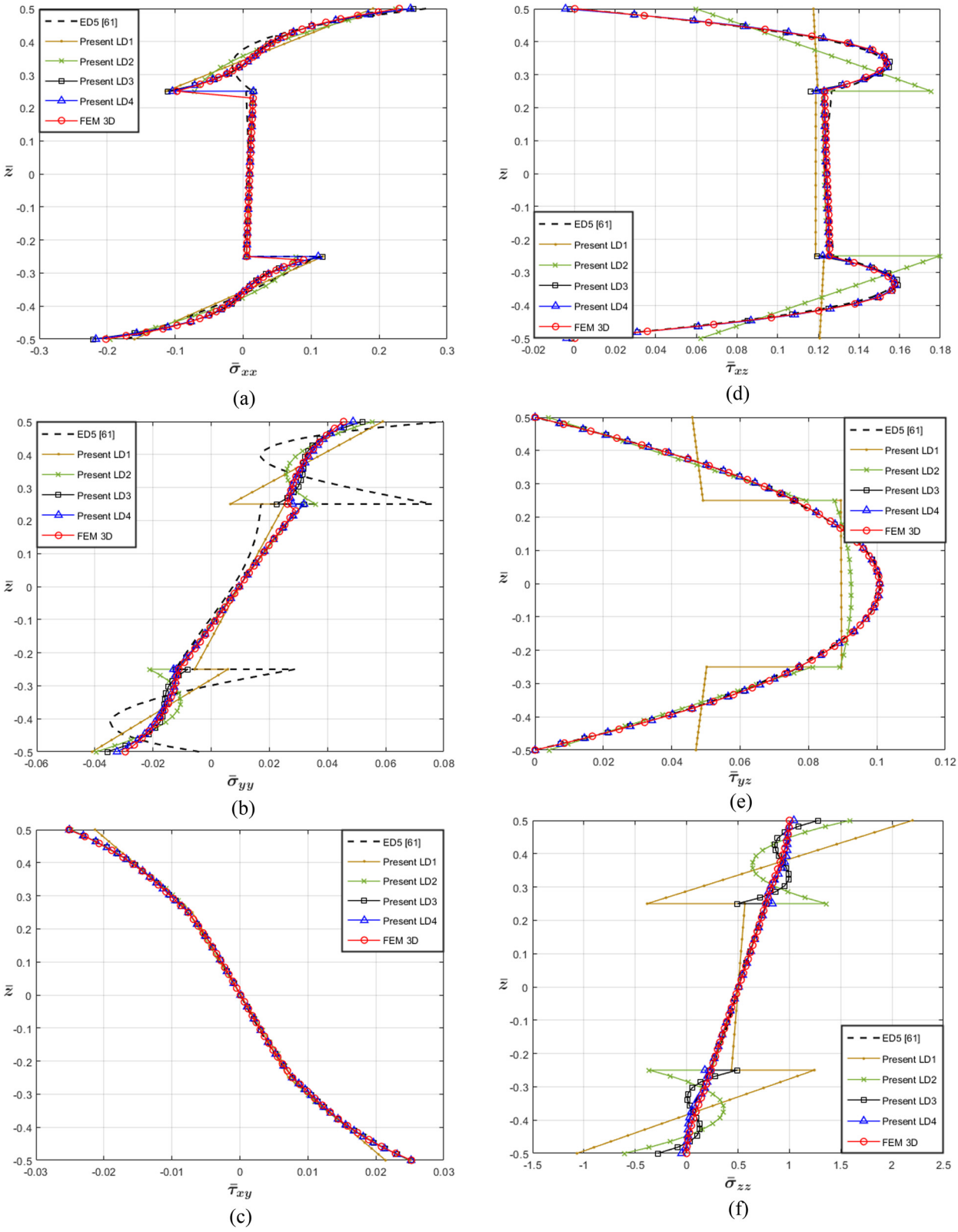

Figure 13: (a)–(f). Problem V. Through-the-thickness variation of stress components at the point $\left(x = \frac{a}{4}, y = \frac{b}{4}\right)$ of a thick case $\left(\frac{a}{h} = 4\right)$.

Table 7: Problem V. Numerical results of displacements and stress components at the point $\left(x = \frac{a}{4},\ y = \frac{b}{4}\right)$ for different values of a/h

a/h	Model	$10^2\bar{u}_{z=\frac{h}{2}}$	$10^2\bar{v}_{z=-\frac{h}{2}}$	$10^2\bar{w}_{z=0}$	$10^2\bar{\sigma}_{xx\,z=\frac{h}{2}}$	$10^2\bar{\sigma}_{yy\,z=\frac{h}{2}}$	$10^2\bar{\tau}_{xy\,z=\frac{h}{2}}$	$10^2\bar{\tau}_{xz\,z=0}$	$10^2\bar{\tau}_{yz\,z=0}$	$\bar{\sigma}_{zz\,z=0}$
4	LD1	−0.255	1.145	1.129	−15.989	5.898	−2.131	11.870	8.957	0.502
	LD2	−0.309	1.258	1.168	−19.578	5.547	−2.480	12.284	9.248	0.503
	LD3	−0.316	1.277	1.189	−22.026	5.211	−2.510	12.396	10.079	0.505
	LD4	−0.316	1.277	1.190	−21.662	4.878	−2.509	12.394	10.084	0.506
	FEM 3D	−0.318	1.284	1.197	−20.190	4.552	−2.513	12.427	10.079	0.507
	ED5 [61]	−0.315	1.267	1.15	−20.359	4.852	−2.488	12.402	10.031	0.508
10	LD1	−0.184	0.520	0.307	−12.879	3.594	−1.281	19.884	2.928	0.500
	LD2	−0.199	0.542	0.320	−12.951	2.474	−1.358	20.339	2.972	0.499
	LD3	−0.199	0.545	0.322	−12.963	2.370	−1.356	20.410	3.218	0.499
	LD4	−0.199	0.545	0.322	−12.975	2.343	−1.356	20.410	3.218	0.499
	FEM 3D	−0.201	0.547	0.324	−12.054	2.212	−1.356	20.482	3.197	0.500
	ED5 [61]	−0.197	0.535	0.314	−12.689	2.316	−1.336	20.552	3.109	0.5
50	LD1	−0.173	0.112	0.079	−7.899	1.523	−0.564	26.452	−0.325	0.497
	LD2	−0.176	0.111	0.080	−7.370	0.970	−0.562	26.926	−0.402	0.497
	LD3	−0.176	0.111	0.080	−7.409	0.966	−0.562	27.137	−0.434	0.497
	LD4	−0.176	0.111	0.080	−7.411	0.961	−0.562	27.137	−0.434	0.497
	FEM 3D	−0.178	0.112	0.082	−7.001	0.923	−0.562	27.166	−0.440	0.500
	ED5 [61]	−0.176	0.111	0.08	−7.375	0.961	−0.56	27.159	−0.439	0.498

presents the numerical results of displacements and stresses for different side-to-thickness ratios. Remarkably accurate solutions are achieved even with low orders such as LD1 or LD2 for thin structures.

3.3 Problem II. Three-layer symmetric square plate

For the second problem, a symmetric cross-ply laminated [0°/90°/0°] square plate constructed from Material 1 is analyzed. Figures 6 and 7 show the through-the-thickness distribution of displacements $(\bar{u}, \bar{v}, \bar{w})$ and all six stress components at the point $\left(\frac{a}{4},\ \frac{b}{4}\right)$ of a thick $\left(\frac{a}{h} = 4\right)$ plate. In Figure 6a, the superior performance of the proposed LW theories is exhibited. Even low-order LW theories like LD1 and LD2 can accurately reproduce the zig-zag effect characteristic of laminated materials, whereas ED5 is unable to capture it. For transversal displacement $\bar{w}$, higher-order models LD3 and LD4 showcase quasi-3D capabilities as indicated by their performance, while ED5 exhibits similar behavior to the present lower-order model LD2. Figure 7(a and b) shows excellent predictive capabilities of LD3 and LD4 throughout the entire thickness direction. Accurate numerical results of displacements and stresses for different side-to-thickness ratios are reported in Table 4. For thicker structures, it is imperative to utilize higher-order models to predict accurately the transversal displacement.

3.4 Problem III. Four-layer symmetric square plate

For the third problem, a symmetric cross-ply laminated [0°/90°/90°/0°] square plate made of material 1 is considered. Figures 8 and 9 show the through-the-thickness distribution of displacements $(\bar{u}, \bar{v}, \bar{w})$ and stress components $(\bar{\sigma}_{xx}, \bar{\sigma}_{yy}, \bar{\tau}_{xy}, \bar{\tau}_{xz}, \bar{\tau}_{yz}, \bar{\sigma}_{zz})$ at the point $\left(\frac{a}{4},\ \frac{b}{4}\right)$ of a thick $\left(\frac{a}{h} = 4\right)$ plate. It is observed that all LW models, including lower-order LD1 and LD2, can capture zig-zag effects in the longitudinal displacement $\bar{u}$. In the case of the $\bar{\sigma}_{yy}$ profile, only higher-order models LD3 and LD4 exhibit excellent agreement with the FEM 3D reference. For out-of-plane distributions, LD3 and LD4 consistently exhibit their superior capability over lower-order models by satisfying free-surface conditions without the need for stress-recovery procedures. Table 5 presents the numerical results of displacements and stresses for different side-to-thickness ratios. Good agreement is obtained for all side-to-thickness ratios presented, *i.e.*, from thick to thin structures.

3.5 Problem IV. Four-layer antisymmetric square plate

For the fourth problem, a symmetric cross-ply laminated [0°/90°/0°/90°] square plate, whose layers are made of material 1, is examined. Figures 10 and 11 show the through-the-thickness distribution of displacements

($\bar{u}$, $\bar{v}$, $\bar{w}$) and stress components($\bar{\sigma}_{xx}$, $\bar{\sigma}_{yy}$, $\bar{\tau}_{xy}$, $\bar{\tau}_{xz}$, $\bar{\tau}_{yz}$, $\bar{\sigma}_{zz}$) at the point $\left(\frac{a}{4}, \frac{b}{4}\right)$ of a moderately thick $\left(\frac{a}{h} = 10\right)$ plate. The results for transversal displacement $\bar{w}$ from both lower and higher-order models surpass those obtained from ED5. Out-of-plane shear stresses $\bar{\tau}_{xz}, \bar{\tau}_{yz}$ are well-reproduced by LD3 and LD4, whereas LD1 and LD2 appear to require a post-processing technique to capture them accurately, particularly in regions where the laminates are rotated 90°. Table 6 presents the numerical results at specific points of displacements and stresses for different side-to-thickness ratios. There are some oscillations for shear stress $\bar{\tau}_{yz}$, the reason is illustrated in Figure 11e where lower-order models are being calibrated as the order of expansion is increased.

3.6 Problem V. Three-layer square sandwich plate

In the final problem, a sandwich [0°/90°/0°] square plate is studied. This specific case was originally presented by Demasi [33] with the consideration of simply-supported boundary conditions applied to all edges. In this work, as mentioned earlier, clamped boundary conditions at all four edges are considered. The thickness of each layer is considered as: $h_{\text{skins}} = 0.25h$ and $h_{\text{core}} = 0.5h$. The two skins ($\varphi = 0°$) are made of material 3 while the core layer ($\varphi = 90°$) is made of material 2. Figures 12 and 13 show the through-the-thickness distribution of displacements ($\bar{u}$, $\bar{v}$, $\bar{w}$) and all six stress components at the point $\left(\frac{a}{4}, \frac{b}{4}\right)$ of a thick $\left(\frac{a}{h} = 4\right)$ plate. As exposed in the earlier cases, the proposed LW theories can accurately capture the zig-zag effect presented in the $\bar{u}$ profile while ED5 struggles. An interesting situation happens in the transversal distribution, where all LW theories reproduce correctly the behavior of the deformation. The difference just lies in the precision of every model. The challenges associated with using ED5 for in-plane stresses ($\bar{\sigma}_{xx}$, $\bar{\sigma}_{yy}$) are evident, as it struggles to accurately trace these profiles. Nevertheless, the advanced higher-order LW models, LD3 and LD4, can accurately predict them. For normal stress $\bar{\sigma}_{zz}$, it is seen that even LD3 fails to reproduce the stress profile at external layers. Therefore, the most reliable option appears to be LD4. The numerical results of displacements and stresses are reported in Table 7. The impact of employing LW theories becomes more evident compared to the previous cases, particularly for thicker configurations.

4 Conclusions

This article deals with the development of LW plate models with quasi-3D capabilities to obtain analytical solutions for the study of cross-ply laminated composite plates with clamped boundary conditions at one or more edges. The CUF is employed to analyze deformation theories of arbitrary order in a systematic manner. The explicit form of the governing equations is derived by substituting the stress-strain and strain-displacement relationships, along with the CUF framework, into the static formulation of the PVD. The boundary-discontinuous double Fourier series methodology is utilized at a layer-level for the very first time to obtain accurate numerical results. The following main conclusions can be drawn:

- By leveraging the versatility of CUF framework, the results indicate that LW theories surpass ESL models in accurately capturing quasi-3D effects, even without including zig-zag terms in the displacement field.
- The convergence analysis shows the strong dependence of the boundary-discontinuous method on the number of trigonometric terms. A more detailed research related to the evaluation of computational cost may be required for a clearer evaluation.
- It is concluded that, unlike ESL models, higher-order LW models such as LD3 and LD4 do not need a post-processing technique to accurately predict the out-of-plane stress distributions. However, if a more precise performance is required, it can be implemented.
- The analytical closed-form solutions based on the LW description, derived through the integration of CUF and the boundary-discontinuous method, entail higher computational costs compared to ESL-based theories. However, their analytical nature makes them highly accurate and valuable for comparison purposes during the product design process.

Future works could include the use of Jacobi polynomials in the displacement field. Another important further research work is the development of mixed theories by employing the RMVT, so the C_z^0 requirements are *a priori* fulfilled.

Acknowledgements: The authors would like to thank the University of Engineering and Technology, Barranco, Peru, for supporting the present work.

Funding information: Authors state no funding involved.

Author contributions: All authors have accepted responsibility for the entire content of this manuscript and consented to its submission to the journal, reviewed all the results and approved the final version of the manuscript. RLW: writing draft, date analysis, editing. JLM: conceptualization, writing, revision.

Conflict of interest: Authors state no conflict of interest.

Data availability statement: The data supporting this study will be made available upon reasonable request.

References

[1] Pagano NJ. Exact solutions for rectangular bidirectional composites and sandwich plates. J Compos Mater. 1970;4(1):20–34.

[2] Pagano N, Hatfield HJ. Elastic behavior of multilayered bidirectional composites. AIAA J. 1972;10(7):931–3.

[3] Ren J. Bending of simply-supported, antisymmetrically laminated rectangular plate under transverse loading. Compos Sci Technol. 1987;28(3):231–43.

[4] Ren J. A new theory of laminated plate. Compos Sci Technol. 1986;26:225.

[5] Ren J. Bending theory of laminated plate. Compos Sci Technol. 1986;27(3):225–48.

[6] Kirchhoff G. Über das gleichgewicht und die bewegung einer elastischen scheibe. J Reine Angew Math. 1850;1850(40):51–88.

[7] Love AEH. A treatise on the mathematical theory of elasticity. Cambridge: Cambridge University Press; 1927.

[8] Reissner E, Stavsky Y. Bending and stretching of certain types of heterogeneous aeolotropic elastic plates. J Appl Mech. 1961;28:402–8.

[9] Reissner E. On transverse bending of plates, including the effect of transverse shear deformation. Int J Solids Struct. 1975;11(5):569–57.

[10] Mindlin RD. Influence of rotatory inertia and shear in flexural motions of isotropic elastic plates. ASME J Appl Mech. 1951;18:1031–6.

[11] Reddy JN. A simple higher-order theory for laminated composite plates. J Appl Mech. 1984;51:745–52.

[12] Murakami H. Laminated composite plate theory with improved in-plane responses. J Appl Mech. 1986;53(3):661–6.

[13] Touratier M. An efficient standard plate theory. Int J Eng Sci. 1991;29(8):901–16.

[14] Li X, Liu D. Generalized laminate theories based on double superposition hypothesis. Int J Num Method Eng. 1997;40:1197–212.

[15] Carrera E. Historical review of Zig-Zag theories for multilayered plates and shells. Appl Mech Rev. 2003;56:287–308.

[16] Reddy J. A generalization of two-dimensional theories of laminated composite plates. Commun Appl Numer Methods. 1987;3:173–80.

[17] Ferreira AJM. Analysis of composite plates using a layerwise theory and multiquadrics discretization. Mech Adv Mater Struct. 2005;12:99–112.

[18] Ferreira AJM, Roque CMC, Jorge RMN, Kansa EJ. Static deformations and vibration analysis of composite and sandwich plates using a layerwise theory and multiquadrics discretizations. Eng Anal Bound Elem. 2005;29:1104–14.

[19] Noor AK, Burton WS, Bert CW. Computational model for sandwich panels and shells. Appl Mech Rev. 1996;49:155–99.

[20] Reddy JN, Robbins DH. Theories and computational models for composite laminates. Appl Mech Rev. 1994;47:147–65.

[21] Noor AK, Burton WS. Assessments of shear deformation theories for multilayered composite plates. Appl Mech Rev. 1989;42:1–18.

[22] Kapania K, Raciti S. Recent advances in analysis of laminated beams and plates. Part 1: shear effects and buckling. AIAA J. 1989;27(7):923–35.

[23] Carrera E. Theories and finite elements for multilayered, anisotropic, composite plates and shells. Arch Comput Methods Eng. 2002;9(2):87–140.

[24] Carrera E. Theories and finite elements for multilayered plates and shells: a unified compact formulation with numerical assessment and benchmarking. Arch Comput Methods Eng. 2003;10:215–96.

[25] Carrera E, Ciuffreda A. A unified formulation to assess theories of multilayered plates for various bending problems. Compos Struct. 2005;69:271–93.

[26] Ferreira AJM, Roque CMC, Carrera E, Cinefra M. Analysis of thick isotropic and cross-ply laminated plates by radial basis functions and a Unified Formulation. J Sound Vib. 2011;330:771–87.

[27] Ramos IA, Mantari JL, Zenkour AM. Laminated composite plates subject to thermal load using trigonometrical theory based on Carrera Unified Formulation. Compos Struct. 2016;143:324–35.

[28] Carrera E, Filippi M, Zappino E. Laminated beam analysis by polynomial, trigonometric, exponential and zig–zag theories. Eur J Mech-A/Solids. 2013;41:58–69.

[29] Carrera E, Cinefra M, Li G. Refined finite element solutions for anisotropic laminated plates. Compos Struct. 2018;183:63–76.

[30] Pagani A, Carrera E, Augello R, Scano D. Use of lagrange polynomials to build refined theories for laminated beams, plates and shells. Compos Struct. 2021;276:114505.

[31] Petrolo M, Augello R, Carrera E, Scano D, Pagani A. Evaluation of transverse shear stresses in layered beams/plates/shells via stress recovery accounting for various CUF-based theories. Compos Struct. 2023;307:116625.

[32] Carrera E, Augello R, Pagani A, Scano D. Refined multilayered beam, plate and shell elements based on Jacobi polynomials. Compos Struct. 2023;304:116275.

[33] Demasi L. Mixed plate theories based on generalized unified formulation Part V:Results. Compos Struct. 2009;88:1–16.

[34] Carrera E, Giunta G. Hierarchical models for failure analysis of plates bent by distributed and localized transverse loadings. J Zhejiang Univ Sci. 2008;9:600–13.

[35] Carrera E, Cinefra M, Petrolo M, Zappino E. Finite element analysis of structures through unified formulation. New Jersey: John Wiley & Sons; 2014.

[36] Carrera E, Giunta G, Brischetto S. Hierarchical closed-form solutions for plates bent by localized transverse loadings. J Zhejiang Univ Sci. 2007;8:1026–37.

[37] Carrera E, Miglioretti F, Petrolo M. Guidelines and recommendations on the use of higher-order finite elements for bending analysis of plates. Int J Comput Methods Eng Sci Mech. 2011;12(6):303–24.

[38] Fazzolari FA, Carrera E. Free vibration analysis of sandwich plates with anisotropic face sheets in thermal environment by using the

Hierarchical trigonometric Ritz formulation. Compos B Eng. 2013;50:67–81.
[39] Ferreira AJM, Carrera E, Cinefra M, Viola E, Tornabene F, Fantuzzi N, et al. Analysis of thick isotropic and cross-ply laminated plates by generalized differential quadrature method and a Unified Formulation. Compos B Eng. 2013;58:544–52.
[40] Chaudhuri RA. On boundary-discontinuous double Fourier series solution to a system of completely coupled P.D.E.'s. Int J Eng Sci. 1989;27:1005–22.
[41] Chaudhuri RA. On the roles of complementary and admissible boundary constraints in Fourier solutions to boundary-value problems of completely coupled rth order PDEs. J Sound Vib. 2002;251(2):261–313.
[42] Chaudhuri RA, Abu-Arja KR. Static analysis of moderately-thick finite antisymmetric angle-ply cylindrical panels and shells. Int J Solids Struct. 1991;28(1):1–15.
[43] Kabir HRH, Chaudhuri RA. A direct Fourier approach for the analysis of thin finite-dimensional cylindrical panels. Comput Struct. 1993;46:279–87.
[44] Chaudhuri RA, Kabir HRH. On analytical solutions to boundary-value problems of doubly-curved moderately-thick orthotropic shells. Int J Eng Sci. 1989;27:1325–36.
[45] Chaudhuri RA, Kabir HRH. Boundary-discontinuous Fourier analysis of doubly-curved panels using classical shallow shell theories. Int J Eng Sci. 1993;31:1551–64.
[46] Chaudhuri RA, Kabir HRH. Sensitivity of the response of moderately thick cross-ply doubly-curved panels to lamination and boundary constraint-I. Theory. Int J Solids Struct. 1993;30(2):263–72.
[47] Chaudhuri RA, Kabir HRH. Sensitivity of the response of moderately thick cross-ply doubly-curved panels to lamination and boundary constraint-II. Appl. Int J Solids Struct. 1993;30:273–86.
[48] Chaudhuri RA, Kabir HRH. Static and dynamic Fourier analysis of finite cross-ply doubly curved panels using classical shallow shell theories. Compos Struct. 1994;28:73–91.
[49] Kabir HRH, Chaudhuri RA. On Gibbs-phenomenon-free Fourier solution for finite shear-flexible laminated clamped curved panels. Int J Eng Sci. 1994;32:501–20.
[50] Chaudhuri RA, Kabir HRH. Fourier solution to higher-order theory based laminated shell boundary-value problem. AIAA J. 1995;33:1681–8.
[51] Chaudhuri RA, Kabir HRH. Effect of boundary constraint on the frequency response of moderately thick doubly curved cross-ply panels using mixed Fourier solution functions. J Sound Vibr. 2005;283:263–93.
[52] Oktem AS, Chaudhuri RA. Higher-order theory based boundary-discontinuous Fourier analysis of simply supported thick cross-ply doubly curved panels. Compos Struct. 2009;89:448–58.
[53] Chaudhuri RA, Kabir HRH. Influence of lamination and boundary constraint on the deformation of moderately thick cross-ply rectangular plates. J Compos Mater. 1992;26:51–77.
[54] Chaudhuri RA, Kabir HRH. A boundary discontinuous Fourier solution for clamped transversely isotropic (pyrolytic graphite) Mindlin plates. Int J Solid Struct. 1993;30:287–97.
[55] Oktem AS, Chaudhuri RA. Levy type analysis of cross-ply plates based on higher-order theory. Compos Struct. 2007;78:243–53.
[56] Oktem AS, Chaudhuri RA. Fourier solution to a thick Levy type clamped plate problem. Compos Struct. 2007;79:481–92.
[57] Oktem AS, Chaudhuri RA. Boundary discontinuous fourier analysis of thick cross-ply clamped plates. Compos Struct. 2008;82:539–48.
[58] Oktem AS, Mantari JL, Soares CG. Static response of functionally graded plates and doubly-curved shells based on a higher order shear deformation theory. Eur J Mech A/Solids. 2012;36:163–72.
[59] Canales FG, Mantari JL. Boundary discontinuous Fourier analysis of thick beams with clamped and simply supported edges via CUF. Chin J Aeronaut. 2017;30(5):1708–18.
[60] Canales FG, Mantari JL. A boundary-discontinuous based Fourier analysis of thick laminated beam via a robust 1D-CUF model. Int J Solids Struct. 2017;118–119:109–18.
[61] Laureano RW, Mantari JL, Yarasca J, Oktem AS, Monge J, Zhou X. Boundary discontinuous fourier analysis of clamped isotropic and cross-ply laminated plates via unified formulation. Compos Struct. 2023;328:117736.
[62] Laureano RW, Mantari JL, Yarasca J, Oktem AS, Zhou X, Hinostroza MA. Closed-form solutions for clamped FGM plates via the unified formulation and boundary discontinuous method. Mech Adv Mater Struct. 2023;1–18. doi: 10.1080/15376494.2023.2261000.

Appendix A

$$
\begin{aligned}
K_{(11)}^{k\tau s} &= J_{55}^{k\tau,zs,z} - J_{11}^{k\tau s}\frac{\partial^2}{\partial x^2} - J_{66}^{k\tau s}\frac{\partial^2}{\partial y^2},\\
K_{(12)}^{k\tau s} &= -(J_{12}^{k\tau s} + J_{66}^{k\tau s})\frac{\partial^2}{\partial x\partial y},\\
K_{(13)}^{k\tau s} &= (J_{55}^{k\tau s,z} - J_{13}^{k\tau,zs})\frac{\partial}{\partial x},\\
K_{(21)}^{k\tau s} &= -(J_{12}^{k\tau s} + J_{66}^{k\tau s})\frac{\partial^2}{\partial x\partial y},\\
K_{(22)}^{k\tau s} &= J_{44}^{k\tau,zs,z} - J_{66}^{k\tau s}\frac{\partial^2}{\partial x^2} - J_{22}^{k\tau s}\frac{\partial^2}{\partial y^2},\\
K_{(23)}^{k\tau s} &= (J_{44}^{k\tau s,z} - J_{23}^{k\tau,zs})\frac{\partial}{\partial y},\\
K_{(31)}^{k\tau s} &= (J_{13}^{k\tau s,z} - J_{55}^{k\tau,zs})\frac{\partial}{\partial x},\\
K_{(32)}^{k\tau s} &= (J_{23}^{k\tau s,z} - J_{44}^{k\tau,zs})\frac{\partial}{\partial y},\\
K_{(33)}^{k\tau s} &= J_{33}^{k\tau,zs,z} - J_{55}^{k\tau s}\frac{\partial^2}{\partial x^2} - J_{44}^{k\tau s}\frac{\partial^2}{\partial y^2}.
\end{aligned}
\tag{A1}
$$

$$
\begin{aligned}
\Pi_{(11)}^{k\tau s} &= J_{11}^{k\tau s}\frac{\partial}{\partial x} + J_{66}^{k\tau s}\frac{\partial}{\partial y},\\
\Pi_{(12)}^{k\tau s} &= J_{66}^{k\tau s}\frac{\partial}{\partial x} + J_{12}^{k\tau s}\frac{\partial}{\partial y},\\
\Pi_{(13)}^{k\tau s} &= J_{13}^{k\tau,zs},\\
\Pi_{(21)}^{k\tau s} &= J_{12}^{k\tau s}\frac{\partial}{\partial x} + J_{66}^{k\tau s}\frac{\partial}{\partial y},\\
\Pi_{(22)}^{k\tau s} &= J_{66}^{k\tau s}\frac{\partial}{\partial x} + J_{22}^{k\tau s}\frac{\partial}{\partial y},\\
\Pi_{(23)}^{k\tau s} &= J_{23}^{k\tau,zs},\\
\Pi_{(31)}^{\tau s} &= J_{55}^{\tau,zs},\\
\Pi_{(32)}^{k\tau s} &= J_{44}^{k\tau,zs},\\
\Pi_{(33)}^{k\tau s} &= J_{55}^{k\tau s}\frac{\partial}{\partial x} + J_{44}^{k\tau s}\frac{\partial}{\partial y}.
\end{aligned}
\tag{A2}
$$